Fabrication of an Aptamer-Functionalised Silica Nanoparticle Construct and its Separation by Magnetic Capture-Hybridisation

Alicja Bulsiewicz

Jesus College
University of Oxford

A thesis submitted for the degree of Master of Science
Trinity Term 2012

Abstract

Fabrication of an Aptamer-Functionalised Silica Nanoparticle Construct and its Separation by Magnetic Capture-Hybridisation

Alicja Bulsiewicz, Jesus College, submitted for the degree of Master of Science, Trinity Term 2012

Nanoparticles produced with surfaces functionalised by highly specific molecular tags are able to target aberrant cells and detect or eliminate them without causing damage to surrounding healthy tissues. Single-stranded DNA (ssDNA) and RNA which fold to form secondary or tertiary structures, termed aptamers, represent a new class of such molecular tags. The nanoparticles, in turn, may carry therapeutic payload or luminescent entities which enable elimination or visualisation of targeted cells respectively.

This project presents fabrication and isolation of a surface-functionalised nanoparticle construct, namely aptamer-tagged silica nanoparticles. DNA aptamers were chosen with the intention to make them useful for clinical or diagnostic applications of targeting neoplastic cells. Indeed, the ssDNA applied here is known to bind mucin-1 which in turn is a biomarker found on the surface of metastatic breast cancer cells. The separation of the construct was made possible by the inclusion of oligonucleotide-bound superparamagnetic particles in the construct; these enabled separation by magnetic capture.

This project investigates two approaches to fabrication of the construct. In the first approach, aptamers, oligonucleotides and magnetic particles are mixed in solution. In the second, silica nanoparticles are functionalised with aptamers, oligonucleotides are bound to magnetic particles and the resulting two parts are hybridised together. The first approach gives higher yields. This may suggest that binding of silica nanoparticles to aptamers may hinder aptamer hybridisation to oligonucleotide fragments, thus resulting in lower construct synthesis yields. However, it is not known yet how the yield changes upon addition of silica nanoparticles into the solution. Therefore, the second experimental approach provides a starting point for fabrication and purification of an anti-cancer drug targeting platform in a simple bench-top setting.

In addition, this thesis discusses the fabrication of silica nanoparticles which were intended to constitute an element of the construct. The work on nanoparticle fabrication aimed to develop a quick and repeatable synthesis method which would result in monodisperse entities. Despite trying various experimental approaches, suitable particles could not be reproducibly obtained. Agglomeration was identified as a major obstacle in the silica nanoparticle production process.

Finally, this project assesses whether the chosen aptamers bind to the metastatic breast cancer cells, which would be necessary if they were to be used for diagnosis or therapy. FACS analysis indeed indicate that ssDNA aptamers attach to the MCF7 cell line, but the optimum conditions for that attachment remain to be determined.

Acknowledgements

First and foremost, I would like to express my thanks and deepest appreciation to my supervisors Prof. Richard Darton and Dr Alex Lubansky for supporting me with their patience and vast knowledge throughout the entire course of my MSc study. Without their expertise and constant encouragement the completion of this multi-disciplinary project could not be possible.

I am equally indebted and grateful to Dr Karl Morten for including me in his research group and guiding me throughout my study. His assistance in this project, expertise and excellent advice were truly invaluable.

It is a pleasure to thank Dr Helen Townley for sharing her experience in the field of nanotechnology and providing mesoporous silica nanoparticles for my project. I am also very grateful to other members of Nuffield Department of Obstetrics and Gynaecology and Begbroke Science Park, especially to Dr Chris Gardener for his help with NanoSight analysis, Rebecca Dragovic for her support with FACS and Dr Janet Carver for her assistance with fluorescence microscopy. I would like to acknowledge Dr Clive Downing and Dr Alison Crossley for producing scanning electron microscope images of silica nanoparticles. I am grateful to Dr Heiko Schiffter for allowing me to use Zetasizer and I would like to acknowledge Begbroke Science Laboratories for making disc centrifuge available to me.

I would like to acknowledge the William Fund for their financial support in funding my experimental work in Nuffield Department of Obstetrics and Gynaecology.

Finally, I would like to thank my parents, grandmother and younger sister for their love and encouragement during the process of writing up this thesis. Most importantly I would like to thank Kuba for his incessant support, motivating me and being amazing at all times.

Declaration

I confirm that this MSc thesis represents my own work. External contributions to the research are acknowledged.

Table of Contents

Abbreviations

- ANB-NOS – (*N*-5-azido-2-nitrobenzoyloxysuccinimide)
- APTES – (3-Aminopropyl)triethoxysilane
- ATCC – American Type Culture Collection
- bp – base pair
- BSA – Bovine Serum Albumin
- DAPI – 4, 6-Diamidino-2-phenylindole dihydrochloride
- DLS – Dynamic Light Scattering
- DMEM – Dulbecco's Modified Eagle's Medium
- FACS – Fluorescence-Activated Cell Sorting
- FBS – Foetal Bovine Serum
- FITC – fluorescein 5(6)-isothiocyanate
- FSC-A – forward scatter
- KCps – kilo Counts per second
- kDa – kilo Dalton
- MCF7 – metastatic breast cancer cell line
- MFI – Mean Fluorescence Intensity
- MRI – Magnetic Resonance Imaging
- MUC-1 – mucin-1
- nm – nanometre
- NP – nanoparticle
- NTA – Nanoparticle Tracking Analysis
- P1 – cell population one
- P2 – cell population two
- PBS – Phosphate Buffered Saline
- PCR – Polymerase Chain Reaction
- PEG – poly(ethylene glycol)
- PEI – polyethyleneimine
- rpm – rounds per minute
- SD – standard deviation
- SELEX – Systematic Evolution of Ligands by EXponential enrichment
- SEM – scanning electron microscopy
- SSC – saline-sodium citrate buffer
- SSC-A – side scatter
- ssDNA – single-stranded DNA
- TEG – triethylene glycol
- TEOS – tetraethyl orthosilicate
- TEM – transmission electron microscopy
- v/v – volume per volume

List of Tables

List of Figures

1 Introduction

This research is concerned with fabricating and purifying a construct which will enable clinicians to locate the sites of cancerous growth in the human body. We can fabricate such a construct using a combination of nanoparticles and biologically active components. In this chapter we introduce the nanotechnology and biology that we will make use of later in the synthesis of the construct and its isolation.

1.1 Nanotechnology and nanoparticles

1.1.1 Nanotechnology

Novel methods of drug delivery using nanoparticles can provide solutions in combating various chronic conditions including cancer, myocardial infarctions or Alzheimer's disease. Functionalised nanoparticles may ideally be applied *in vivo* for diagnosis and therapy.

The particles supplied by nanotechnology come in a variety of sizes, structures and surface properties. They have demonstrated potential as drug delivery vehicles, contrast agents or biosensors (Smith *et al*., 2006). Alexis *et al*. (2008) described a size range of nanomaterials used in nanotechnology as 1 to 100 nm in, at least, one dimension. The materials which are found within this range have distinctive characteristics encountered only at the nanoscale level (Sakamoto *et al*., 2010). Faraji and Wipf (2009) determined the potential of nanotechnology in provision of therapeutic dosing through targeted therapies, possible intracellular zone for nanoparticle protection from degradation and efflux as well as establishment of sustained-release drug profiles.

Nanotechnology plays an increasing role in biotechnology, biomedical sciences and engineering (Smith *et al*., 2006) by supplying tools to support targeting of diseased tissues as well as separation and purification of biomaterials in a fast, efficient and cheap manner. For

instance, nanoparticles may be utilised for delivery of therapeutic drugs to malignant tumours (Levy-Nissenbaum *et al*., 2008), as molecular diagnostics or for *in vivo* imaging (McCarthy and Weissleder 2008). Generally, a requirement in nanoparticle design is to provide entities able to remain sufficiently long in the patient's circulation and indicate a disease location (Hallmark *et al*., 2010). Furthermore, their strengths include large surface to volume ratio and small size which play a crucial role in facilitating *in vivo* drug delivery (McCarthy and Weissleder 2008). Nanoparticles should be able to target malignant tissues selectively and show minimal non-specific binding to healthy cells. In order to be efficient in lesion eradication, they should neither agglomerate nor be endocytosed by components of the patient's immune system (Hallmark *et al*., 2010).

There are various types of nanoparticles which find application in therapy and diagnosis. Faraji and Wipf (2009) identified seven particle types used in biomedical research and drug delivery, namely inorganic, polymeric, solid lipid nanoparticles as well as liposomes, nanocrystals, nanotubes and dendrimers.

1.1.2 Silica nanoparticles

Silica or silica-coated nanoparticles have been frequently employed in biomedical research due to their lack of harmful side-effects. Mader *et al*. (2008) attributed the potential of silica nanoparticles to its various advantages such as availability in many sizes and size distributions, affordability, fairly good biocompatibility and sufficient surface reactivity to ensure an ease of its functionalisation (Smith *et al*., 2006). The surface of silica can be easily modified by coupling with various functional groups, for instance: amino, thiol or carboxyl (Smith *et al*., 2006). Furthermore, the attachment of biological molecules like monoclonal antibodies or DNA sequences is easy. Consequently, silica particles conjugated to biorecognition molecules find applications as sensors or in biomarker discovery (Berezovski

et al., 2008). According to Santra *et al*. (2001) silica nanoparticles are easy to centrifuge and are hydrophilic due to the presence of silanol groups, so it is not difficult to suspend them in aqueous solutions. Furthermore, silica nanoparticles are resistant to both aqueous and nonaqueous solvents, are nontoxic and can be easily functionalised (Santra *et al*., 2001).

1.1.3 Fabrication of silica nanoparticles

Smith *et al*. (2006) recognised two approaches towards fabrication of nanoparticles, namely: top-down and bottom-up. The former uses mechanical degradation processes of bulk materials to obtain nanoparticles. However, the drawbacks of this methodology are poor reproducibility as well as no control over particle sizes and shapes. In the bottom-up approach, the nanomaterials are fabricated by atom-by-atom self-assembly. In this way, more elaborate structures can be produced. The major limitation of this methodology is the not fully understood synthesis process (Smith *et al*., 2006).

Silica nanoparticles can be synthesised by the Stöber process (Rao, *et al*., 2005) or, alternatively, by the reverse microemulsion method (Bagwe *et al*., 2004). The former method is frequently adopted for synthesis of colloidal particles with diameters below 100 nm. Alternatively, a reverse micelle method (also known as water-in-oil (W/O) microemulsion technique) may be employed for silica nanoparticle synthesis (Bagwe *et al*., 2004). It has the disadvantage of a longer duration (1-2 days) in comparison to the Stöber technique. On the other hand, it produces highly spherical and monodisperse nanoparticles (Knopp *et al*., 2009).

1.1.4 Functionalisation of silica nanoparticles

Silica nanoparticles must have functionalised surfaces in order to be effective tools in bioimaging, biochemical analysis, in photonics or nonlinear optical materials (Bagwe *et al*., 2004). The functionalisation of silica nanoparticles with fluorophores such as FITC or Alexa dyes enables fast and simple detection of fluorophore-tagged entities in complex biological

environments. Moreover, many luminescent molecules may be incorporated inside the silica nanoparticles which protects them from the damaging impact of surroundings, thus providing excellent signal amplification (Bagwe *et al*., 2004). Also, the absorption and emission spectra of fluorophore-functionalised particles do not shift significantly from the native fluorophore spectra which is an advantage during detection (Knopp *et al*., 2009). Despite these advantages, there are several drawbacks to fluorophore usage. These include excessive brightness, poor photostability or interference with binding of other molecules to the surface of the silica nanoparticles (Knopp *et al*., 2009).

Silica nanoparticle surface functionalisation is a necessary step when challenged with agglomeration problems. Xu *et al*. (2003) hypothesised that the tendency of silica nanoparticles to form agglomerates may arise from interparticle hydrogen bonding. In that case, the modification of nanoparticle surface with PEG remedied the obstacle. This could be attributed to prevention of direct contact between particles because of PEG polymer chains extending into solution. Li and Kaner (2005) identified agglomeration as a serious dilemma in examination of nanoparticle properties. Similarly to Xu *et al*. (2003), the agglomeration was attributed to mutually attractive interactions between particles such as: van der Waals forces or chemical bonding. The suggested solution was to use mechanical agitation. However, this proved only to enforce the agglomeration phenomena. Thus, addition of surfactants at high enough concentrations was identified as a possible remedy (Li and Kaner, 2005).

1.1.5 Magnetic nanoparticles

Magnetic nanoparticles constitute yet another type of nanoparticle. Especially those made of iron oxide, have found applications in tissue repair, MRI, cellular therapy, drug delivery and magnetic separations (McCarthy and Weissleder, 2008). Their major advantages are the tuneability of sizes (5-500 nm), obedience to Coulomb's law (thus capability of being

manipulated by external magnetic field gradient) and large surface area which facilitates attachment of biological molecules such as DNA or proteins (Tartaj *et al*., 2005). On the other hand, the major limitations of iron oxide core magnetic particles are their tendency to agglomerate and inclination to biodegradation (Knopp *et al*., 2009). Also, they can be toxic towards a biological system when used *in vivo*, especially when doped with cations such as Mg, Fe, Co or Ni (Veiseh *et al*., 2010). A common method of addressing agglomeration and toxicity has been to provide a protective coating (e.g. PEG, dextran, chitosan or PEI) at the surface of the nanoparticles (Veiseh *et al*., 2010). Additionally, this outer layer can be functionalised with biomolecules which, in turn, may facilitate recognition of target entities (Knopp *et al*., 2009).

1.1.6 Magnetic separation

Magnetic nanoparticles have found applications in magnetic separations - versatile and well-established methods for separating biological entities (e.g. cells, DNA or proteins) bound to magnetic tags (Furlani *et al*., 2007). The uses of magnetic separations include cell sorting, protein purification and removal of unwanted entities from suspensions (Whitesides *et al*., 1983). Materials employed as magnetic labels in such separations are, for instance, iron oxide core superparamagnetic nanoparticles which are attracted to a source generating magnetic field. In this way, the entities conjugated to magnetic particles can be separated from dilute suspensions.

Furlani *et al*. (2007) identified two approaches towards magnetic separation, direct and indirect. The former involves application of magnetic particles which have surfaces functionalised with molecules (e.g. antibodies or aptamers) to recognise their targets in the solution. Alternatively, an indirect approach is used, which involves an incubation of the target molecule with a primary antibody, and only after successful binding between these

entities takes place, the magnetic particles (with surfaces functionalised with secondary antibodies) are introduced into a solution. As the secondary antibodies have high affinities towards the primary antibodies, a conjugation occurs. In both of these approaches a magnetically-bound material is separated from solution upon application of an external magnetic field (Furlani *et al*., 2007).

Magnetic separations can be carried out with the use of microfluidic systems. However, an application of magnetic nanoparticles in such endeavours is only at its preliminary stage (Lund-Olsen *et al*., 2007). Despite the novelty of these systems, several research groups employ them in their work on magnetic separations which utilise magnetic nanoparticles with or without conjugated biological entities. Examples include Hallmark *et al*. (2008) and Darton *et al*. (2009) who manufactured capillary arrays which were used for investigation of the capture of superparamagnetic nanoparticles by an externally applied magnetic field. Similarly, Lund-Olsen *et al*. (2007) examined the behaviour of DNA oligonucleotide-functionalised magnetic beads in a fluidic setup under the influence of an electromagnet. Finally, Lou *et al*. (2009) combined usage of magnetic beads and microfluidic separation chip to achieve a ssDNA aptamer selection This process was termed M-SELEX.

The skilfully purified surface-functionalised nanoparticles separated magnetically from the unbound entities can act as tools for medical treatment. In order to achieve this, detailed information about the disease to be targeted is needed. Without this knowledge the nanoparticles may fail to target cells of interest and thus cause elevated toxicity to the patient. Novel nanoparticle-based drug delivery strategies can be applied in targeting such chronic conditions as cancer.

1.1.7 Magnetic capture-hybridisation

Magnetic capture-hybridisation is a method applied frequently for detection of DNA or RNA. It applies magnetic particles bound to nucleic acids for isolation of complementary DNA or RNA sequences from heterogeneous solutions (Hornes and Korsnes, 1990). This technique was found to be very effective in the detection of pathogenic microorganisms from various sources such as cell lysates or food matrices (Bach *et al.*, 1999 and Amagliani *et al.*, 2005). Major strengths of magnetic capture-hybridisation include low cost, speed of detection and simplicity. Magnetic capture-hybridisation reduces significantly number of steps and time required for detection and isolation of nucleic acids. Therefore, it challenges classical DNA or RNA purification methods such as phenol-chloroform extractions, precipitations or CsCl density gradient centrifugation (Bach *et al*., 1999).

1.2 Cancer

1.2.1 Molecular basis of cancer

Cancer is a disease of multicellular organisms and arises through abnormal proliferation of cells within an organism. This, in turn, is caused either by a variety of alterations within the DNA sequence of a cell (genetic change) or by permanent modification of the gene expression pattern (epigenetic change) (Ruddon, 2007).

Tumours or neoplasm can be divided into benign and malignant forms. The former is characterised by cell proliferation at a particular location in a body. This type of lesion can be eradicated by surgical excision or local irradiation quite effectively. However, when a tumour becomes malignant, the cells start proliferating uncontrollably, crossing the basal lamina, detaching themselves from primary disease sites and travelling through circulation to invade secondary locations. The neoplasm which exhibits this feature is termed a cancer and its

invasive activity is referred to as metastasis. Once tumour cells embark on metastasising, the condition becomes incurable for 90% of patients (Alberts *et al*., 2008).

Alberts *et al*. (2008) ascribe cancer occurrence to only a few slowly-dividing cancer stem cells capable of infinite multiplication and self-renewal. The development of neoplasm is enhanced by the ability of cancer cells to ignore normal signalling mechanisms operating within the healthy tissues. In this way, order between cells is disrupted and tumour enlarges. This may be achieved by production of fast-replicating layers of cells, maintaining support from connective tissue (stroma) and angiogenesis. This last process (defined as formation of new blood vessels) plays a key role in supplying a growing tumour with nutrients and oxygen. When neoplasm attains a certain size (usually about 1 or 2 mm), the conditions inside it become hypoxic. Consequently, pro-angiogenic signals are generated which enhance formation of new blood capillaries. However, these are mostly leaky, tortuous and have many dead-ends and aberrant underlying basement membrane (Alexis *et al*., 2008). As a result cancer tissue keeps sending signal proteins, such as VEGF (vascular endothelial growth factor), which act in propagating capillary formation (Alberts *et al*., 2008). These biomolecules may serve as important targets for anti-cancer treatments.

1.2.2 Biomarkers

Apart from indefinite self-renewal and capability of ignoring normal signalling mechanisms, the cancer cells may be differentiated from healthy entities by the presence of so-called biomarkers. These are measurable indicators of cellular states and are recognised as signatures for tracking cancerous lesions (Berezovski *et al*., 2008). Biomarkers encompass a variety of biomolecule types, for instance hormones, DNA molecules, oncogenes, glycoproteins or DNA modifications (Tothill, 2009). They may be aberrantly expressed and displayed on the cell membrane. Their occurrence indicates the development of the cancerous state. Several

biomarkers have been discovered so far, such as: PSA (prostate cancer), CEA (pancreatic cancer), CA72-4 (gastric carcinoma), MUC-1 (breast cancer) and many others (Tothill, 2009).

1.2.3 Mucin-1

MUC-1 (mucin-1) is a glycoprotein which is found on the apical surface of epithelial cells of many human organs. Its aberrant glycosylation and overexpression on cell surfaces has been associated with biomarking cancer development (Ferreira *et al*., 2006). Structurally it is a large, rod-like glycoprotein that consists of three distinct regions. The first one is an N-terminus filament protruding from the cell surface and made of variable numbers of peptide tandem repeats (VNTR). These, in turn, contain amino acids such as serine, threonine as well as proline, where serines and threonines are post-translationally modified with *O*-linked oligosaccharides. Overall, carbohydrate chains constitute about 50% of mucin mass (Ferreira *et al*., 2009). The further two sections of MUC-1 are the transmembrane region and C-terminus cytoplasmatic tail (Da Pieve *et al*., 2009). Mucin-1 is known to be characteristic to several types of cancer which arise from epithelial cells, e.g. prostate, breast, ovary, colon, pancreas and lung (Ferreira *et al*., 2009). Mucin-1 has a therapeutically useful feature of being recycled by cell organelles (endosomes, Golgi apparatus). Therefore, mucins may act as entry portals for molecules which specifically bind to them (Ferreira *et al*., 2009).

The cancer environment is favourable to nanoparticle accumulation due to the phenomenon of passive targeting. However, a more effective method of directing nanoparticles to the diseased cells is active targeting. This can be realised by nanoparticle surface functionalisation with ligands which, in turn, bind specifically to targets such as cancer biomarkers. The ligands which enhance targeting are antibodies, oligopeptide-based molecules, folate-based molecules, affibodies, nanobodies and aptamers.

1.3 Aptamers

1.3.1 Aptamer structure and function

Aptamers are short, usually 20-80 monomers (6 to 26 kDa), single-stranded DNA and RNA sequences or their modified analogues (Levy-Nissenbaum *et al*., 2008). Since the development of techniques for their selection, these nucleic acid sequences have had an increasing impact on biotechnology, nanotechnology and medicine. They may rival monoclonal antibodies in providing better therapies to cancer. The term aptamer has been applied to peptide sequences as well (Baines and Colas, 2006).

Nucleic acids are known for their role in storage and transfer of genetic material (Pestourie *et al*., 2005). However, single-stranded nucleic acids can also form both secondary and tertiary structures (Phillips *et al*., 2008). It is this three-dimensional conformation (not base-base complementarity) which allows specific target binding (Sampson, 2003). De-los-Santos-Alvarez *et al*. (2008) identified a number of tertiary structures adopted by single-stranded nucleic acids upon attachment to their ligands. These are: hairpin, G-quartet, stem-bulge, pseudoknot and T-junction. In this way, aptamers are able to couple to a variety of targets, for instance: coagulation factors, hormones, inflammation markers, cells, peptides, small molecules (e.g. ATP), nucleic acids or even perform catalysis of chemical reactions (Brody and Gold, 2000 and Pestourie *et al*., 2005). Moreover, several aptamers are used for binding to cancer-related targets such as: MUC-1, VEGF, PSMA, HER-3 or RET (Levy-Nissenbaum *et al*., 2008).

1.3.2 Aptamer modifications

If aptamers are to be effective tools in biomedical applications, they must be made resistant to enzymatic or chemical cleavage upon introduction to the systemic circulation. DNA and RNA sequences are vulnerable to disintegration due to nuclease action, thus a set of modifications

needs to be implemented in order to improve their stability and efficacy (Lee *et al*., 2006). Three approaches towards decreasing aptamer susceptibility to nucleolytic attack have been tested so far: modifications to nucleotide bases, phosphodiester backbone and introduction of Spiegelmers (enantiomeric aptamers) (Sampson, 2003).

1.3.3 Aptamers versus monoclonal antibodies

The ability of aptamers to bind molecular targets with high affinity and specificity makes them suitable candidates for therapeutic as well as diagnostic applications. They show much resemblance to widely used monoclonal antibodies (Lee *et al*., 2006). Both types of biomolecules have dissociation constants for their targets in nanomolar or picomolar range and they attach to species of interest by folding into three-dimensional conformations based on their sequence (Nimjee *et al*., 2005). Despite the huge success of monoclonal antibodies in daily molecular biology routine and proven potential in therapy, aptamers offer a few advantages which make them more attractive choices for medical applications. First, they are smaller than monoclonal antibodies, only 10-20 kDa in comparison to 150 kDa, thus can penetrate diseased tissues more effectively (Alexis *et al*., 2008). Moreover, monoclonal antibodies show batch-to-batch variation. On the other hand, once aptamers are fabricated, the same sequence may be produced by chemical synthesis repeatedly. Furthermore these nucleic acids, as opposed to antibodies, are less immunogenic, allow introduction of various modifications to the sequence and renaturate to their original conformations after high temperature treatment (Nimjee *et al*., 2005).

1.3.4 Aptamers as therapeutics and diagnostics

Aptamers have been successfully applied in therapy and diagnosis. The most illustrious example is an anti-vascular endothelial growth factor (anti-VEGF) RNA aptamer known as

pegaptanib sodium and marketed under name of Macugen® (Ng *et al*., 2006). It is used for treatment of neovascular age-related macular degeneration (AMD). Other examples of aptamers raised for biomedical applications include TTA1-^{99m}Tc modified RNA aptamer attached to nuclear-imaging tracer isotope ^{99m}Tc generated against tenascin-C and used for its detection, A10 aptamer conjugated to nanoparticles and applied to target prostate-specific membrane antigen (Levy-Nissenbaum *et al*., 2008), phototoxic DNA aptamers used for targeting MUC-1 (Ferreira *et al*., 2009) or Spiegelmers against ghrelin (a peptide hormone) (Lee *et al*., 2006).

1.4 Project Aims

The aim of this project is to purify aptamer-functionalised silica nanoparticles from a solution of unbound entities by the magnetic capture-hybridisation method. In order to achieve this objective, the full construct (aptamer-modified silica nanoparticles hybridised to oligonucleotide fragment bound to superparamagnetic particles) needs to be fabricated. First, solid (non-porous) silica nanoparticles will be obtained and characterized by various methods. Upon successful synthesis of these nanoparticles a surface functionalisation with fluorophore-containing DNA aptamers will be performed and the full construct will be fabricated by hybridisation through an attached superparamagnetic particle (see Figure 1). Finally, the constructs will be isolated using a magnetic field. The hybridisation of aptamer-functionalised silica nanoparticles to superparamagnetic particles will be investigated by the measurement of fluorescence intensity. If fabrication, surface-functionalisation and isolation of solid silica nanoparticles are successful, these experiments will be repeated with mesoporous silica nanoparticles.

The findings of this investigation should demonstrate the usefulness of aptamer-silica nanoparticle constructs in targeting metastatic breast cancer cells.

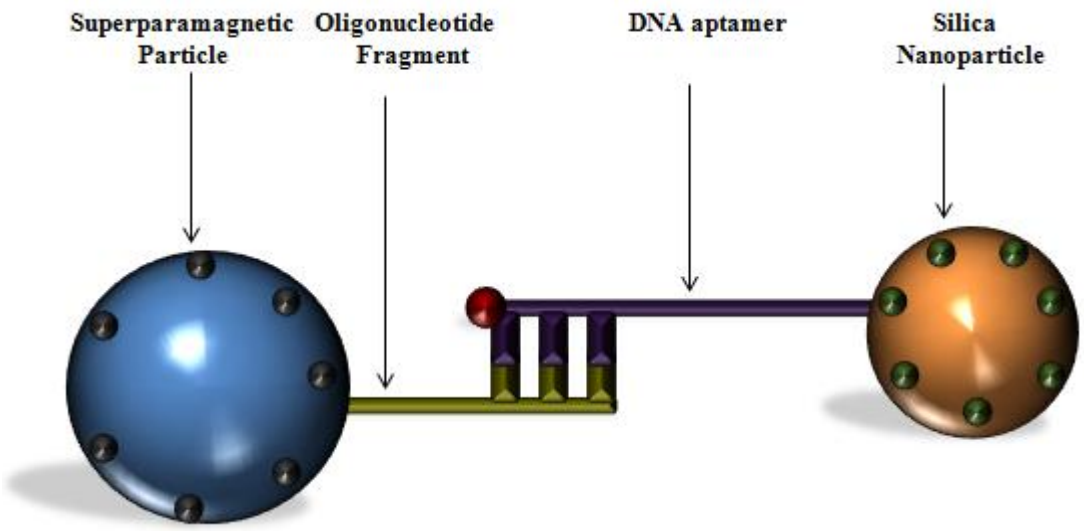

Figure 1 Diagrammatic representation of aptamer-functionalised silica nanoparticles bound to superparamagnetic particles by oligonucleotide fragment. A blue sphere represents superparamagnetic particle, orange sphere represents silica nanoparticle, yellow rod – oligonucleotide fragment, purple rod – aptamer, grey spheres – streptavidin residues, green spheres – FITC fluorophores and red sphere – ATTO647N fluorophore.

2 Materials and Methods

2.1 Materials

2.1.1 Reagents and solvents

The reagents and solvents were purchased from Sigma-Aldrich (Sigma-Aldrich Company Ltd., Poole, UK) unless otherwise stated. Foetal bovine serum (FBS) was acquired from PAA The Cell Culture Company (PAA Laboratories Ltd., Yeovil, UK). The ssDNA aptamer sequences (Ferreira, *et al*., 2009) were bought from Eurogentec (Eurogentec S.A., Liege, Belgium). The synthesised 70 base long sequence was:

5'-GAGACAAGAATAAACGCTCAAGAAGTGAAAATGACAGAACACAACATT CGACAGGAGGCTCACAACAGGC-3'. Glyceryl was bound to the 3' end of the ssDNA sequence and ATTO647N fluorophore was conjugated to the 5' end.

The purified DNA oligonucleotide sequence necessary for hybridisation was purchased from Eurogentec (Eurogentec S.A., Liege, Belgium). The synthesised 21 base long sequence was: 5'-TTGAGCGTTTATTCTTGTCTC-3'. This oligonucleotide fragment was modified at the 3' end with Biotin TEG (Biotin attached to oligonucleotide sequence with 15 atom long triethylene glycol spacer).

2.1.2 Cell line

The human metastatic breast cancer cells (MCF7) and Chinese Hamster Ovary cells were obtained from ATCC (American Type Culture Collection, Manassas, VA, USA) and were used throughout this project.

2.2 Construct Fabrication Methods

2.2.1 Synthesis of solid silica nanoparticles

Monodisperse, 60 nm, uniform-size silica nanoparticles were synthesized in a stepwise manner (Rao, *et al*., 2005). First, 36.8 ml absolute ethanol and 20.3 ml deionised water were poured into a beaker, which, in turn, was placed in a sonication bath. After 10 minutes, 0.3 ml of 98% (v/v) tetraethyl orthosilicate (TEOS) was added in a dropwise manner with a pastette. Second, after 20 minutes, 54.4 ml of 28% (v/v) ammonium hydroxide was added as a catalyst to speed up the condensation reaction. Sonication was continued for another 60 minutes until a white turbid suspension was observed. Both steps were conducted at room temperature. The indicated substrate volumes were used in the initial experiments and were changed later (see Table 2).

2.2.2 Synthesis of mesoporous silica nanoparticles

The mesoporous silica nanoparticles were synthesised with the use of a base-catalysed sol-gel hot aqueous solution as described by Hom *et al.* (2010). 100 mg of cetyltrimethylammonium bromide was dissolved in 48 ml water and 350 µl 2 M sodium hydroxide. The resultant solution was heated to 80°C. Subsequently, 0.5 ml of TEOS was added to the solution containing cetyltrimethylammonium bromide surfactants. After 15 min, 127 µl of 42% (v/v) 3-(trihydroxysilyl)propyl methylphosphonate were added into the mixture and the solution

was stirred for 2 h. The resultant particles were centrifuged and washed with methanol. The cetyltrimethylammonium bromide surfactants were removed from the pores by dispersing the particles in solution of 20 ml methanol and 1 ml of 12.1 M hydrochloric acid and refluxing the mixture for 24 h. The particles were then washed with ethanol. Subsequently, 5 mg of nanoparticles were dispersed in a solution of 2.5 mg PEI and 1 ml absolute ethanol, stirred for 30 min and washed with ethanol and deionised water (Hom, *et al.* 2010).

2.2.3 Conjugation of FITC to APTES

In order to make silica nanoparticles fluorescent we needed to attach fluorescent moiety to the surface of the nanoparticles. 100 µl of (aminopropyl)triethoxysilane (APTES) and 25 mg of fluorescein 5(6)-isothiocyanate (FITC) were mixed together in 5 ml absolute ethanol in a dry nitrogen atmosphere. The components were stirred magnetically for 12 hours and were protected from light by coverage with aluminium foil. The resulting solution was stored in a 5 ml Falcon tube in a refrigerator at 4ºC.

2.2.4 Coating of silica nanoparticles with FITC-APTES

60 nm silica nanoparticles were diluted in 2.5 ml deionised water and poured into a small glass vessel. The glass vessel was placed inside a beaker filled with deionised water, which, in turn, was placed in the sonication bath. A separate solution was prepared from 2.25 ml absolute ethanol to which 130 µl of tetraethyl orthosilicate (TEOS) had been added together with 130 µl of FITC-APTES. After 10 minutes of sonication the FITC-APTES solution was added to the sonicating silica nanoparticles. 100 µl of 28% (v/v) ammonium hydroxide was added to catalyse the reaction. Sonication continued for another 15 minutes. After completion of sonication, the small glass vessel was removed from the bath, and the silica nanoparticles were centrifuged and washed twice in deionised water to remove any unbound FITC. The nanoparticles were stored at 4ºC in a refrigerator, in deionised water. The fluorescence of

these silica nanoparticles was checked on the fluorescence spectrophotometer to verify that the coating had formed.

2.2.5 Fluorescence microscopy

The presence of MUC-1 biomarkers on the surface of metastatic breast cancer cells (MCF7) was determined with the use of a Leitz DMRBE fluorescent microscope. Before analysis on the microscope, MCF7 cells were treated with nuclear stain, DAPI, in mounting medium (Vector Laboratories) in order to find out if cells can internalise it.

Subsequently, the cells were incubated with primary MUC-1 antibody – monoclonal mouse anti-human CD227, clone BC-2 (Serotec). In order to visualise the cells the fluorescent secondary antibody was utilised - FITC-conjugated donkey anti-mouse IgG (Jackson ImmunoResearch Laboratories). The images of MCF7 cells were captured with a Hamamatsu Orca C4742-95 digital camera using Openlab software (Improvision).

2.2.6 Fluorescence spectrophotometry

The fluorescence intensities of ATTO647N and FITC fluorophores attached to aptamers and silica nanoparticles respectively was determined with the use of fluorescent spectrophotometer. The system applied was Varian Cary Eclipse Fluorescent Spectrophotometer (Varian, Inc, Walnut Creek, CA, USA). A disposable polycarbonate cuvette with 100 µl of FITC-bound silica nanoparticles in 3 ml of deionised water was placed inside a fluorescence spectrophotometer. A monochromator was set to provide a wavelength of light suitable to excite the fluorophores Fluorescence emission spectra for FITC-bound silica nanoparticles were recorded with the use of Cary Eclipse software. The same procedure was applied for fluorescence determination of aptamer-functionalised silica nanoparticles.

2.2.7 Aptamer binding to mesoporous silica nanoparticles

0.5 ml of mesoporous silica nanoparticles in a 1.7 ml Eppendorf tube were span down in the centrifuge for 5 minutes at the speed of 15,000 rpm. After the spin the supernatant was taken off from the Eppendorf tube with a pipette and discarded. The remaining nanoparticles were washed by addition of 1 ml of water to the tube and spinning the contents in centrifuge for 5 minutes at the speed of 15,000 rpm. After removal of supernatant, 1 ml of DMEM medium was added to the nanoparticles. The nanoparticles were mixed with the medium with a pipette. Afterwards, 10 µl of 100 µM aptamers were added to the solution. The solution was again mixed with the pipette. The Eppendorf tube was attached to a spinning wheel which was left in the fridge (4°C) overnight. On the following day, the nanoparticles with aptamers were span down in a centrifuge for 5 minutes at 15,000 rpm. Medium was removed with the pipette. 1 ml of PBS was added to the tube and the contents were mixed with the pipette. Afterwards, aptamers with nanoparticles were taken for analysis on spectrophotometer or plate reader.

2.2.8 Hybridisation

Hybridisation buffer was made (6X SSC, 1% SDS, 0.1% Tween 20) to facilitate binding between two DNA sequences. The buffer was warmed up to 37°C in order to solubilise it. Hybridisation buffer was pipetted into a few Eppendorf tubes (depending on experiment). Aptamer solution was added to the final concentration of 67 nM or 100 nM. Subsequently, oligonucleotide solution (without silica nanoparticles) was added to the solution (final concentrations depended on experiment). Eppendorfs were attached to rotating cylinder in the oven set to 50°C for 60 min. After recovery from the oven, 100 µl of sample was taken for fluorescence intensity analysis and returned to the tube after completed analysis. This method was also followed for hybridisation of aptamer-functionalised mesoporous silica nanoparticles

to oligonuleotide fragments. However, various volumes (5 – 50 μl) of aptamer-functionalised mesoporous silica nanoparticles were added to the hybridisation solutions during this investigation. Also, final concentrations of oligonucleotide fragments added to hybridisation solutions ranged between 1 – 1100 nM.

2.2.9 Plate reader

Two BMG Labtech Fluorescence Microplate Readers were used for measurement of fluorescence intensity of ATTO647N fluorophores attached to DNA aptamers. Initially FLUOstar Optima was used (gains 2900 and 2800). FLUOstar Omega was used (gain 3500) for examination of aptamer-functionalised mesoporous silica nanoparticles.

96-well black plates were used to analyse the fluorescence intensity of ATTO647N functionalised aptamers. Each well was filled with 100 μl of sample.

2.2.10 Magnetic concentration

Magnetic Particle Concentrator (Dynal MCP – E) for microtubes of Eppendorf type (Oslo, Norway) was used for separation of paramagnetic particles with attached oligonucleotides, aptamers and solid or mesoporous silica nanoparticles (the type of silica nanoparticles was used depending on experiment). After recovering Eppendorfs with full constructs (paramagnetic particle, oligonucleotide, aptamer, silica nanoparticle) from oven after hybridisation, the samples were put in the magnetic concentrator for 15-20 minutes. Subsequently, supernatant was removed and taken for fluorescence analysis. The paramagnetic particles were washed with wash buffer 1X SSC, 0.1% SDS and tubes were left for 15 minutes at room temperature. After that time the wash buffer 1 was removed and taken for analysis. Next, wash buffer 2 (0.1X SSC, 0.1% SDS) was added to the beads and the

sample was felt for 15 minutes at room temperature. Afterwards, the supernatant was removed and taken for analysis. Another wash buffer was added to the beads (2X SSC, 0.1% SDS) and the tubes were put in the oven set to 40°C for 15 minutes. Next, supernatant was removed from the tubes and taken for analysis, whereas wash buffer 2 was added to beads and they were put in the oven set to 40°C for 15 minutes. Finally, the supernatant was removed and 100 µl of hybridisation buffer was added to the beads. The beads were resuspended in hybridisation buffer and taken for analysis.

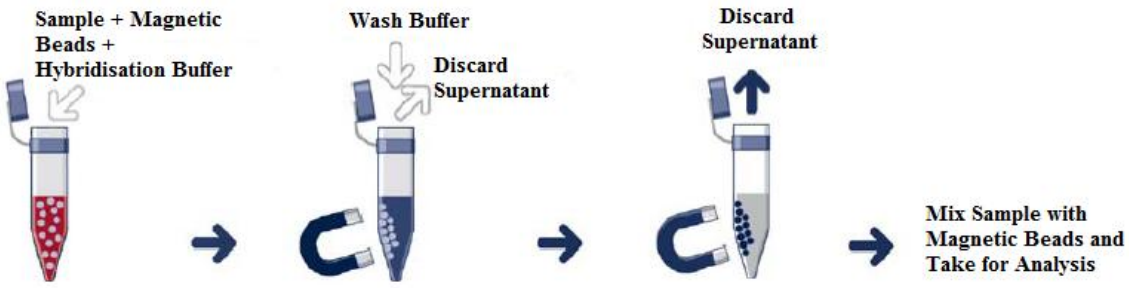

Figure 2 Diagrammatic representation of magnetic–capture hybridisation method. The full construct is placed in hybridisation buffer (the first tube). The second tube represents washing of superparamagnetic beads which were attracted by the permanent magnet. After washes, the last wash buffer is removed (the third tube). Finally, a new volume of buffer is added, permanent magnet is removed and the resuspended sample is taken for analysis. (Adapted from Berensmeier (2005)).

2.3 Size and Charge Characterisation Methods

2.3.1 Disc centrifugation

The size distributions of silica nanoparticles were determined with the use of a disc centrifuge (CPS Disc Centrifuge) by the differential sedimentation method. This instrument can detect nanoparticles sized between 5 nm and 75 µm.

First, the gradient was established by injecting 1.6 ml of varying volumes of 24% w/v and 8% w/v sucrose solutions. Subsequently the gradient was sealed with 0.1 ml of dodecane. Second, the nanoparticle samples were injected (0.1 ml each). The speed of the centrifuge was set to 24000 rpm or 12000 rpm (depending on experimental requirements).

2.3.2 Scanning Electron Microscopy (SEM)

A Scanning Electron Microscope was used to analyse uncoated silica particles and measure their diameters. The microscope applied for this purpose was JEOL 840F equipped with cold cathode field emission gun. Its operating voltage was between 0.5 and 40 kV. Silica particles were dropped onto a polished aluminium stub and dried. Then, the nanoparticles were coated with 2 nm of platinum in the following way. A sputter coater bombarded a platinum target with argon atom, so that platinum atoms were ejected from the target by the ionised gas and deposited on the sample surface. The applied accelerating voltage was 5 kV.

2.3.3 Zetasizer

The sizes and size distributions of silica nanoparticles were determined with the use of dynamic light scattering (DLS) system (Zetasizer 3000 HS, Malvern Instruments Ltd, Malvern, UK) with a 532 nm laser. Deionised water was filtered through 0.2 μm filters before the experiments started. 100 μl of the nanoparticle suspension were diluted with 3 ml of filtered deionised water in a transparent polycarbonate cuvette to avoid multiscattering events. Particles present in the water were illuminated by a beam of light from the laser. Autocorrelation functions were calculated and analysed using the DTSv1.56 software provided by Malvern. Measurements were done in triplicate with eight runs each at 25ºC for determination of the mean hydrodynamic diameter of the nanoparticles in suspension.

2.3.4 Zeta potential

The zeta potential of the silica nanoparticles was determined by Zetasizer Nano ZS (Malvern Instruments Ltd, Malvern, UK) by a combination of laser Doppler velocimetry and phase analysis light scattering (patented technique termed M3-PALS). Preceding the experiment, a 3 ml of pH 3 aqueous solution was mixed with 100 μl of silica nanoparticles in a glass vial.

Next, the resultant solution was taken up with 10 ml syringe and injected into a disposable capillary cell. The cell was equipped with two outlets which were closed with two fitting plugs. Subsequently, the cell was placed inside Zetasizer for analysis. The measurements were done in triplicate with ten runs each at 25ºC for determination of zeta potential of the silica nanoparticles. After recovery of disposable capillary cell from the Zetasizer, the subsequent zeta potential measurements were done for the silica nanoparticles suspended in pH 4, pH 5, pH 5.5, pH 6, pH 6.5, pH 7, pH 7.5, pH 8 and pH 9 aqueous solutions.

2.3.5 NanoSight analysis of nanoparticle sizes

The size and size distribution of silica nanoparticles were determined with the use of NanoSight NS500 system. The particle detection range of this instrument instrument is between 10 nm and 1000 nm. Nanoparticles were diluted in 5 ml PBS, so that the overall dilution was 1 in 1000. The samples were illuminated with a 75 mV laser at 405 nm. The size determination of a sample was based on Nanoparticle Tracking Analysis (NTA) which is a new technique for rapid, real-time visualisation and analysis of nanoparticles in liquid medium. During examination, the sample was illuminated with a beam of light from the laser and the particles within the scattering volume could be observed moving under Brownian motion. The NTA programme identified and tracked the centre of each particle individually on frame-by-frame basis throughout the length of a video (usually 900 frames or 30 seconds). From this information, the distance a particle travelled in x or y direction was automatically calculated and translated into particle diffusion coefficient. This, in turn, was utilized in estimating the particle hydrodynamic diameter.

2.4 Cell Culture and Analysis Methods

2.4.1 Cell line maintenance

The MCF7 cells were maintained in 175 cm^2 flasks and grown in a Dulbecco's Modified Eagle's Medium (DMEM) supplemented with 10% (v/v) FBS, L-glutamine and penicillin/streptavidin. Passaging (splitting a cell culture into new flasks) was performed on a 4-5 day basis. Experiments in this project were performed with cell cultures grown to 80% - 90% confluency.

2.4.2 Immunohistochemistry

This procedure was developed in order to detect mucin-1 on the surface of MCF7 cells. A 4-well plate with 0.5 ml of MCF7 cells (which reached confluency) in medium was recovered from an incubator. Fine-end pastettes were used to collect the medium (the cells remained attached to glass coverslips at the bottom of the wells). The cells were washed with PBS twice. PBS was removed and 400 µl of fixation solution (formalin solution 10% neutral bufferd) was added into each well and the plate was left for 5 minutes. The fixation solution was removed by pastette and the cells were washed twice with PBS. After removal of PBS, 0.5 ml of a blocking solution (3% BSA v/v in PBS) was added into each well. The plate was left for 30 minutes. Subsequently, an anti-MUC-1 primary antibody (antibody: monoclonal mouse, anti-human CD227, clone BC-2 (Serotec)) solution was prepared (4 µl of antibody in 200 µl, 0.1% BSA v/v in PBS) and loaded into each well. The coverslips were lifted carefully from the antibody solution and placed on clingfilm in a wet box (a small plastic box with a wet tissue inside). A 50 µl sample of the primary antibody solution was loaded on each coverslip and allowed to spread to give a uniform layer on top of the cells on the coverslip. The coated coverslips were left for 1 hour at room temperature. After 1 hour the coverslips were washed with 0.1% BSA v/v in PBS solution for 5 minutes thrice. In the meantime a solution of secondary antibody was prepared (5.3 µl donkey anti-mouse FITC-labelled in 400

µl 0.1% BSA v/v in PBS solution (Jackson ImmunoResearch Laboratories)). The secondary antibody was protected from the light with an aluminium foil. The secondary antibody was applied to form a thin layer on the coverslips (which were placed in a wet box) and these were left for 1 hour at room temperature. After 1 hour, the coverslips were washed in the same manner as in the case of the primary antibody. The coverslips were recovered from PBS and placed (with their coated side down) on a glass slide (two coverslips on one slide). Under each coverslip a drop of mounting solution was placed which contained DAPI (4,6-diamidino-2-phenyl-indole, dihydrochloride (Vector Laboratories)). DAPI is a blue dye which was used in the fluorescent microscopy to visualise nuclei. The cells labelled with antibody were visualised with the fluorescent microscope.

2.4.3 Fluorescence-activated cell sorting (FACS)

A flow cytometer (Becton Dickinson LSRII) was used to determine aptamer attachment to metastatic breast cancer cells (MCF7). A 633 nm red laser beam was directed through a hydrodynamically-focused stream of MCF7 cells in solution of 0.5% FBS (v/v) in PBS. The flow cytometer was equipped with a 670/14 bandpass filter to pick up the signal from the ATTO647N fluorophore which was attached to the aptamer.

2.4.4 Aptamer binding to MCF7 cells

The MCF7 cells were grown in two 4-well plates in a 37ºC incubator until the cells formed confluent lawn. The cells were recovered from the incubator and medium was removed from each well with a pastette. The cells were washed twice with PBS in order to remove cell debris. Subsequently, 200 µl of 80 µg/ml BSA w/v in PBS was pipetted into each well in

order to block the cell surface from non-specific binding. Aptamer solution was added in precise amounts so as to obtain concentrations of 100 nM, 10 nM, 1nM in wells numbered 1, 2, 3 in the first and the second 4-well plates. No aptamers were added to the forth well. Next, the first 4-well plate was incubated on ice at 4ºC for 1.5 hour and the second 4-well plate was incubated at 37ºC for 30 minutes. After incubation the 4-well plates were recovered and MCF7 cells were treated with a few drops of trypsin in order to remove them from the wells. 1 ml 4% v/v FBS in PBS was added into each well to stop trypsin activity. The cells were mixed by pipette and poured into Eppendorf tubes. The Eppendorf tubes were span down in the centrifuge at 1200 rpm for 5 minutes. After recovery from the centrifuge, the supernatant was removed with a pipette and again 1 ml of FBS with 4% v/v in PBS was added. The whole procedure was repeated twice. Finally, after recovery from the centrifuge the cells were resuspended in 0.5% FBS v/v in PBS. The samples were taken for FACS analysis.

3 Results

3.1 DNA Aptamer – Silica Nanoparticle Construct Synthesis and Characterisation

3.1.1 Characterisation of silica nanoparticles

Three batches of silica nanoparticles were synthesised by the modified Stöber method. The aim was to obtain nanoparticles which would show a narrow size distribution. 60 nm was the target diameter of nanoparticles in all the batches. Both batch 1 and 2 were fabricated so that the volume of water was 20.3 ml as opposed to batch 3 in which water volume was 5.4 ml. The volumes of substrates used for synthesis of batch 1 and 2 were referred to as old ratio. Whereas, the name used for substrate volumes in batch 3 was new ratio (Table 1).

Table 1 Substrate volumes used for synthesis of old ratio and new ratio solid silica nanoparticles.

Substrate	Old ratio [ml]	New ratio [ml]
Ethanol	36.8	46.6
H_2O	20.3	5.4
TEOS	0.3	0.3
NH_4OH	54.4	47.7

Table 2 Comparison of three batches of solid silica nanoparticles visualised by SEM. All columns represent silica nanoparticles which were not coated with aptamers. The first and second column (from the left) show solid silica nanoparticles synthesised by old ratio volumes of substrates. The last column represents solid silica nanoparticles fabricated with new ratio of substrate volumes. All batches show variability in size and morphology. The aggregation of silica nanoparticles can be clearly observed in batch 2 particles.

Sample	Uncoated silica particles (old ratio, batch 1)	Uncoated silica particles (old ratio, batch 2)	Uncoated silica particles (new ratio)
SEM images	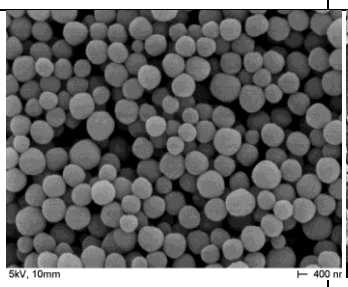	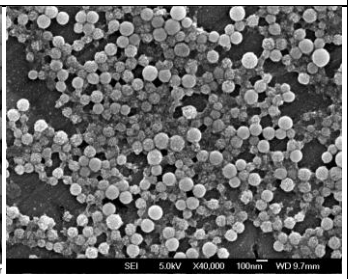	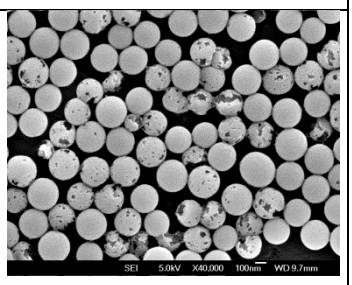
	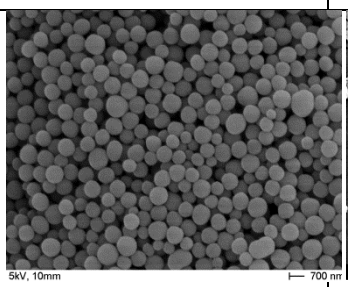	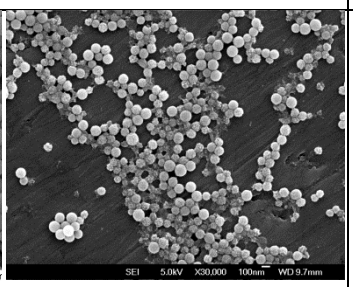	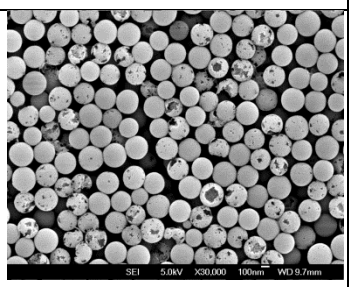
	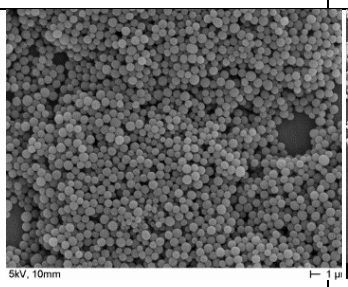	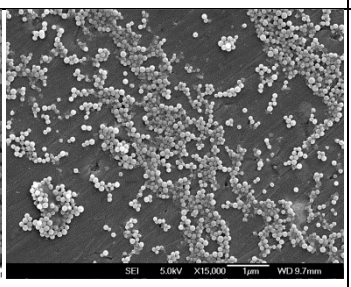	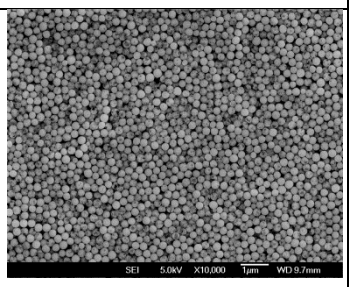
Mean particle diameter [nm]	162	116	215
SD [nm]	26	15	20

Table 2 compares three batches of solid silica nanoparticles. It can be observed that all batches resulted in larger particle diameters than was expected from results presented by Rao *et al.* (2005). The SEM image of batch 1 revealed that the nanoparticles had 162 nm in diameter with a standard deviation of 26 nm. Batch 2 produced aggregated and smaller nanoparticles (116 nm) than batch 1 particles.

A SEM image of batch 3 silica nanoparticles (new ratio) was completely different from batch 1 and batch 2. The particles were more uniformly-sized than the previously fabricated samples and were not aggregated. However, their size was over 200 nm. Also, many particles were hollow inside which made their structure fragile and resulted in breaking.

Mesoporous silica nanoparticles (provided by Dr Townley) were analysed by TEM. It could be seen that these particles were comparable in size to batch 2 solid silica nanoparticles but they were not aggregated (compare with Table 2).

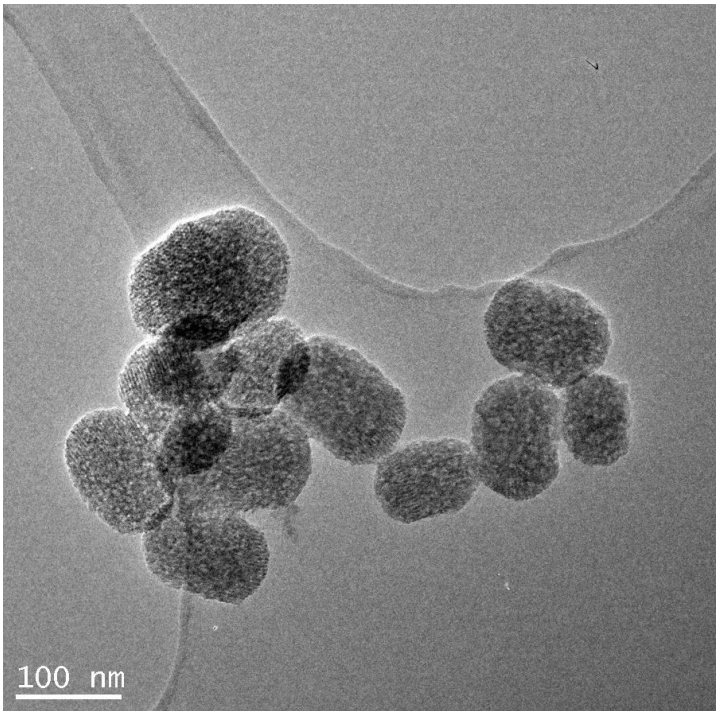

Figure 3 TEM image of uncoated mesoporous silica nanoparticles. A mean diameter of nanoparticles was 113 nm and standard deviation (SD) was equal to 16 nm.

The SEM images of solid silica nanoparticles were comparable with NanoSight images of batch 2 (Figure 4) and batch 3 (Figure 5). The SEM indicated that the diameter of batch 2 silica nanoparticles was around 116 nm (for these nanoparticles which could be observed as separate entities in the aggregate) and NanoSight demonstrated a comparable peak of 110 nm. The smaller peaks of 208 nm and 335 nm must have indicted the aggregates.

Similarly, the highest peak obtained from NanoSight for new ratio particles (batch 3) was equal to 256 nm which was comparable to that measured by SEM (215 nm). The two smaller peaks observed on NanoSight image (92 nm and 126 nm) may have indicated the pieces of broken particles.

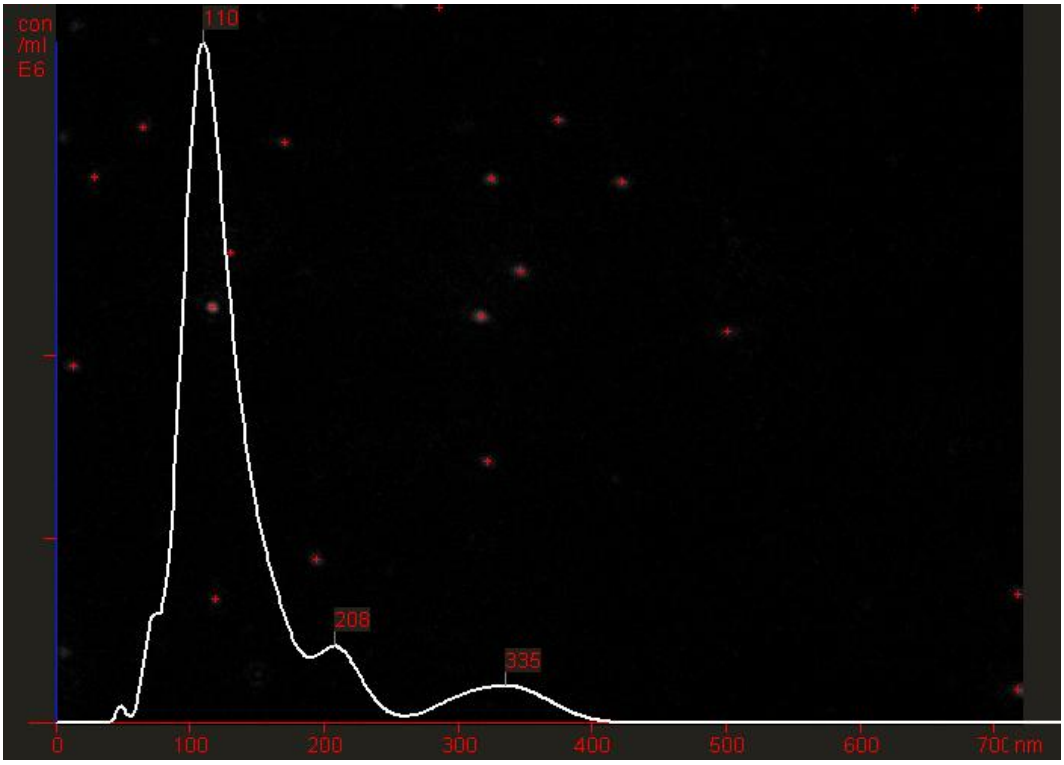

Figure 4 Size distribution of uncoated silica nanoparticles (old ratio, batch 2). The three peaks (110, 208, 335) indicate the three most frequently encountered sizes of silica nanoparticles in the investigated sample. The x-axis corresponds to silica nanoparticle diameters. The y-axis corresponds to the concentration of silica nanoparticles in the given sample.

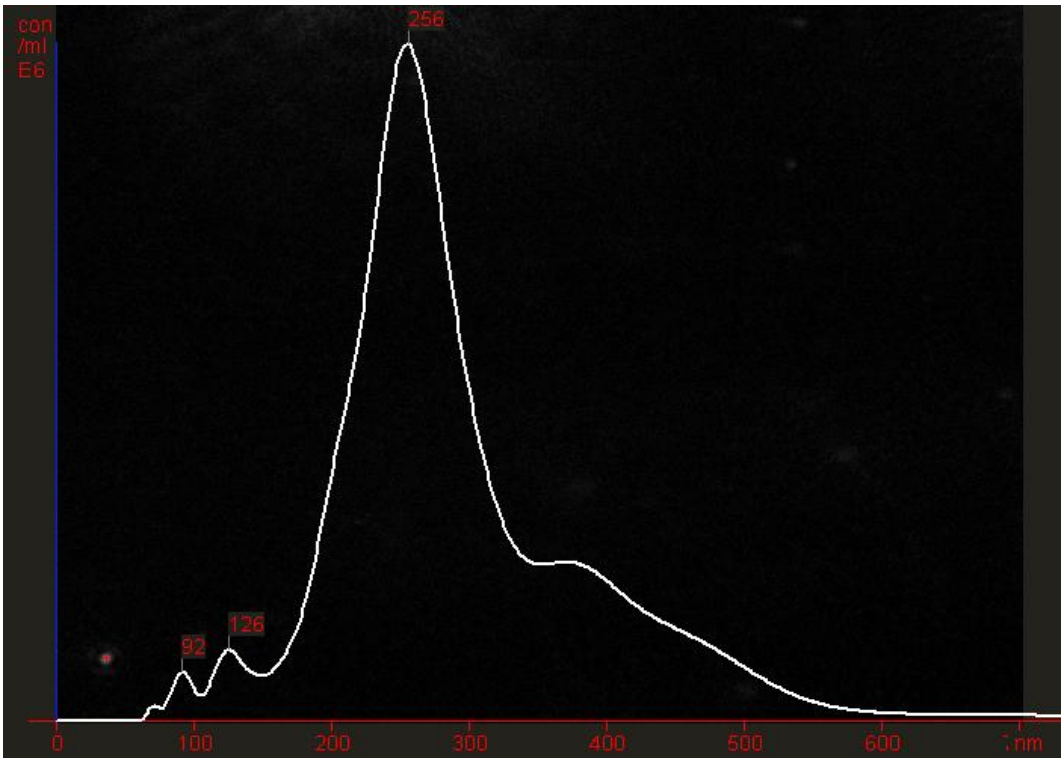

Figure 5 Size distribution of uncoated silica nanoparticles (new ratio). The three peaks (92, 126, 256) indicate the three most frequently encountered sizes of silica nanoparticles in the investigated sample. The x-axis corresponds to silica nanoparticle diameters. The y-axis corresponds to the concentration of silica nanoparticles in the given sample.

The Zetasizer study demonstrated that solid silica nanoparticles synthesised by the new ratio volumes gave sizes of around 300 nm. On the other hand, according to the Zetasizer readings, the old ratio (batch 2) particles ranged between 200 and 260 nm in diameter (Table 3). These results for new ratio nanoparticles are higher than the SEM and NanoSight outcomes.

Similarly to the new ratio particles, the Zetasizer readings for particles synthesised by old ratio volumes gave larger diameters. The higher diameters of the old and new ratio particles were ascribed to formation of aggregates between particles which resulted in larger diameter readings.

Table 3 Zetasizer size measurements of uncoated solid silica nanoparticles. Two types of nanoparticles were analysed: new ratio volumes and old ratio batch 2. Both samples were measured three times by Zetasizer.

Test number	New ratio		Old ratio (batch 2)	
	Size [nm]	Standard deviation [nm]	Size [nm]	Standard deviation [nm]
1	299.2	0.9	263.9	2.8
2	295.6	3.4	197.7	10.0
3	291.4	2.0	262.2	14.5

The final measurement technique used to identify the silica nanoparticle diameters was disc centrifugation. All three batches of solid silica nanoparticles were investigated with this method and showed comparable results. The disc centrifuge readings for batch 1 indicated the presence of a large peak of 20-70 nm and a smaller peak of 100-250 nm (Figure 6).

The disc centrifuge image of batch 2 also gave two peaks: a larger one of 30-100 nm and a smaller of 150-300 nm (Figure 7).

The final disc centrifuge picture of new ratio silica nanoparticles also showed two peaks: a larger one of 30-70 nm and a smaller one of 200-300 nm (Figure 8).

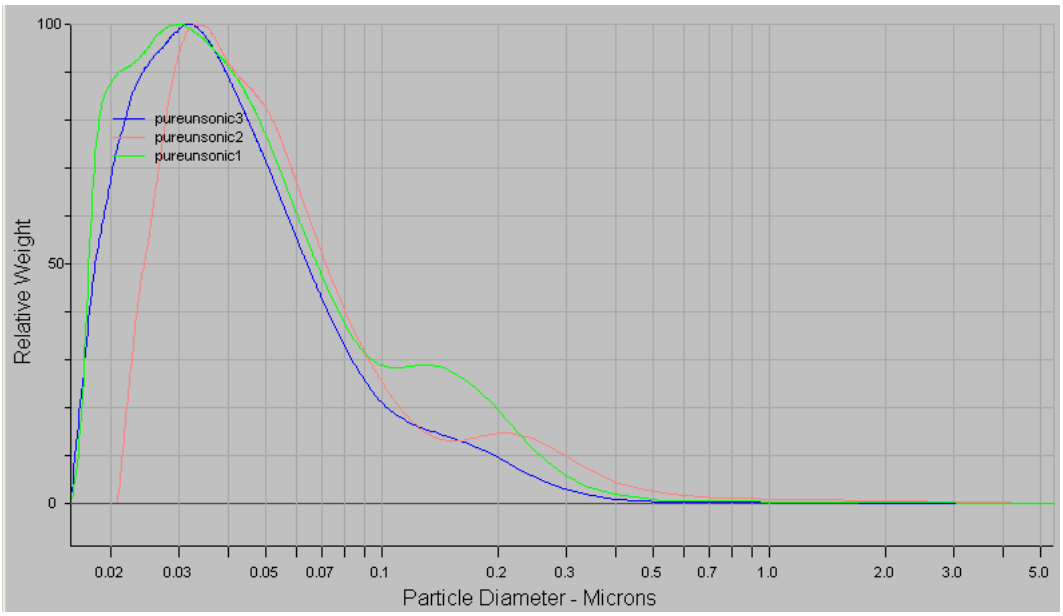

Figure 6 Size distribution of uncoated solid silica nanoparticles (old ratio substrate volumes, batch 1) measured by disc centrifuge. The sample was measured three times and each measurement is represented by different line colour (pink, green, blue). The x-axis corresponds to particle diameter in µm, whereas y-axis corresponds to relative weight of silica nanoparticles. Rotational speed of the disc centrifuge was 24,000 rpm.

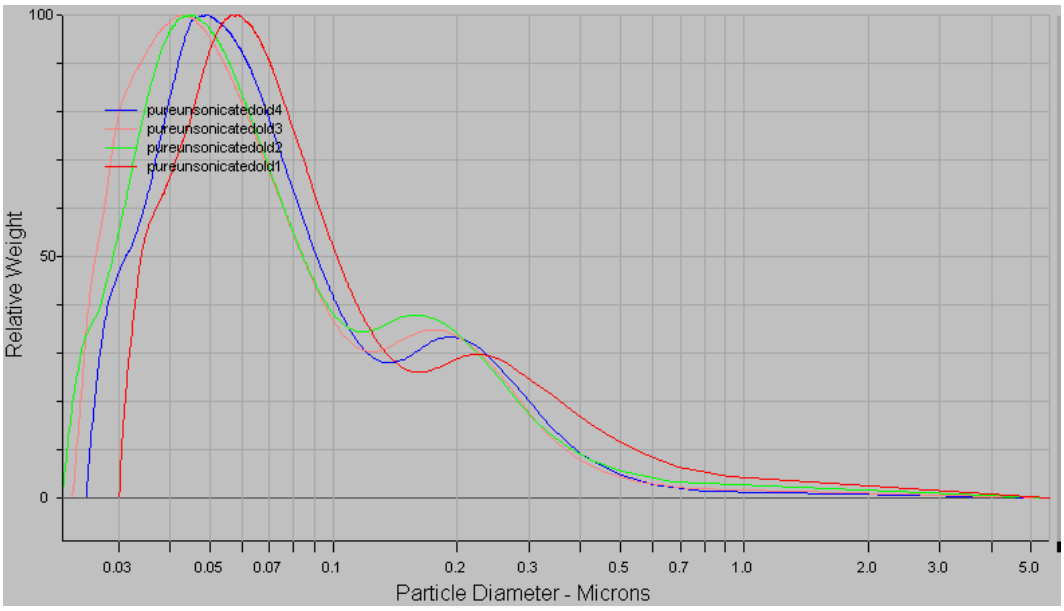

Figure 7 Size distribution of uncoated solid silica nanoparticles (old ratio substrate volumes, batch 2) measured by disc centrifuge. The sample was measured four times and each measurement is shown as different line colour (red, green, blue and pink). The x-axis corresponds to particle diameter in µm, whereas y-axis corresponds to relative weight of silica nanoparticles. Rotational speed of the disc centrifuge was 24,000 rpm.

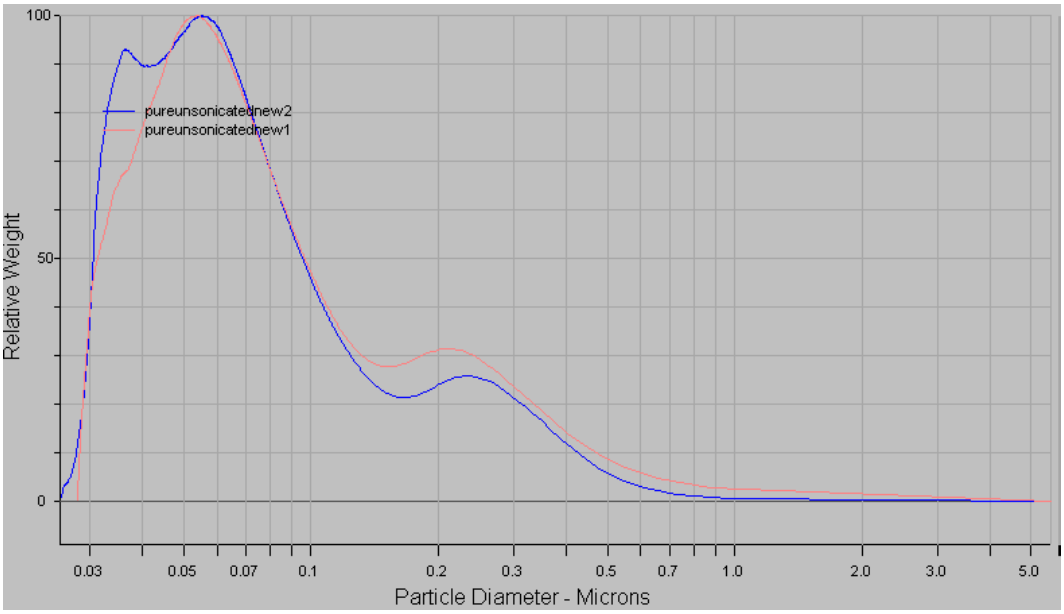

Figure 8 Size distribution of uncoated solid silica nanoparticles (new ratio substrate volume) measured by disc centrifuge. The sample was measured two times and each measurement is shown as different line colour (red and blue). The x-axis corresponds to particle diameter in µm, whereas y-axis corresponds to relative weight of silica nanoparticles. Rotational speed of the disc centrifuge was 24,000 rpm.

3.1.2 Approaches to prevent aggregation of silica nanoparticles

Silica nanoparticles are negatively charged in aqueous solutions at pH 7, so they should have repelled each other and formed monodisperse entities. However, based on Zetasizer (see Table 3) and disc centrifuge results as well as the SEM outcome for batch 2 (Table 2), attractive interactions between solid silica nanoparticles were suspected. Thus, it became necessary to exclude the possibility of agglomeration due to electrostatic interactions. SEM samples of solid silica nanoparticles (batches 1 and 3) as well as the TEM images of mesoporous silica nanoparticles showed separately formed entities but could not determine whether these nanoparticles were agglomerated (Table 2 and Figure 3). On the other hand, batch 2 of solid silica nanoparticles showed clear aggregation (Table 2). Therefore, zeta potential of solid silica nanoparticles synthesised by the new ratio volumes was measured in order to determine at which pH values the

silica nanoparticles tended to agglomerate. The pH of solutions used in this study ranged between pH 3 and pH 9. The data indicated (Figure 9) that the colloidal dispersion of solid silica nanoparticles was most stable, thus not aggregated, between pH 5 and pH 8 when zeta potential ranged between -50 to -60 mV. At pH values below 5 and above 8, the zeta potential indicated lower stability of nanoparticle dispersion, thus showing the tendency of nanoparticles to agglomerate. As solutions used in this project had pH of around 7, thus silica nanoparticles should not have agglomerated. However, further investigations were undertaken in order to determine if nanoparticle agglomeration occurred.

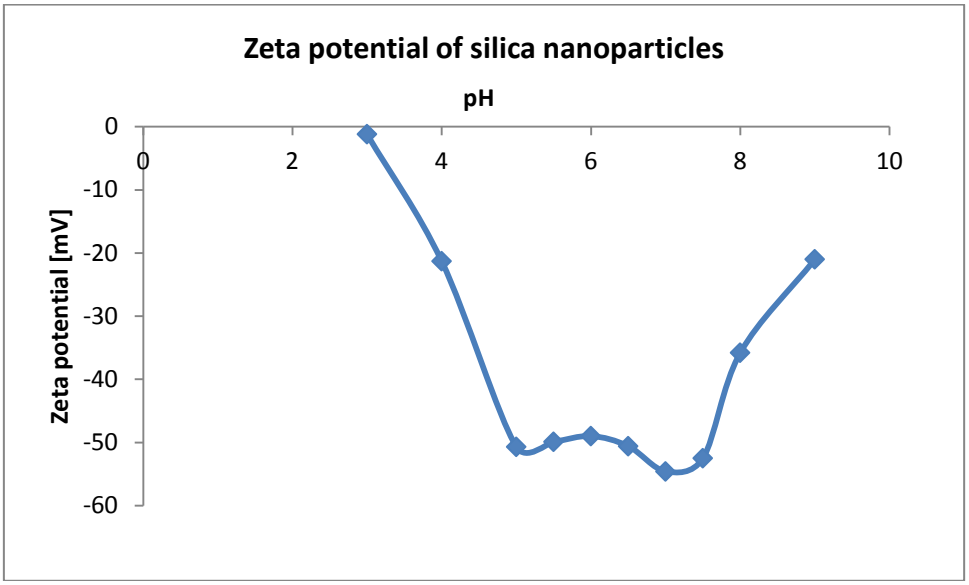

Figure 9 Zeta potential of uncoated solid silica nanoparticles (new ratio substrate volumes). The x-axis corresponds to pH, whereas y-axis corresponds to zeta potential in mV. Experimental conditions under which the zeta potential was measured are given in Table A.7 in the Appendix.

The first approach to address a suspected agglomeration of nanoparticles was to add a BSA protein to the nanoparticle containing solution. NanoSight was applied in order to investigate whether addition of BSA caused any alteration in the silica nanoparticle size readings. It was thought that BSA as a positively charged molecule would be attracted by negatively charged silica nanoparticles and in this way coat them and protect them

from interactions with other silica nanoparticles. However, this investigation proved to be inconclusive as BSA increased the background noise and made reading of the results more difficult. There was also the suspicion that BSA forms aggregates with silica nanoparticles. The sonication of BSA containing samples did not solve the agglomeration question either, as large aggregates continued to form (data not shown).

The second approach which was applied to address the question of agglomeration was the examination of the silica nanoparticles by disc centrifuge. Furthermore, the disc centrifuge was used to investigate the effect of sonication on particle size as well as to compare consequences of applying various rotational speeds to nanoparticles.

Figures 10 and 11 show sonicated and not sonicated silica nanoparticle samples respectively. These measurements indicate that there was no significant difference in size between the samples. This may be due to high rotational speed of the disc centrifuge (24,000 rpm) which might have caused disruption of agglomerates. Both disc centrifuge pictures showed two peaks: 30-70 nm and 150-300 nm. The two particle sizes can be seen on the SEM images (Table 2), confirming the measurements of Figures 10 and 11.

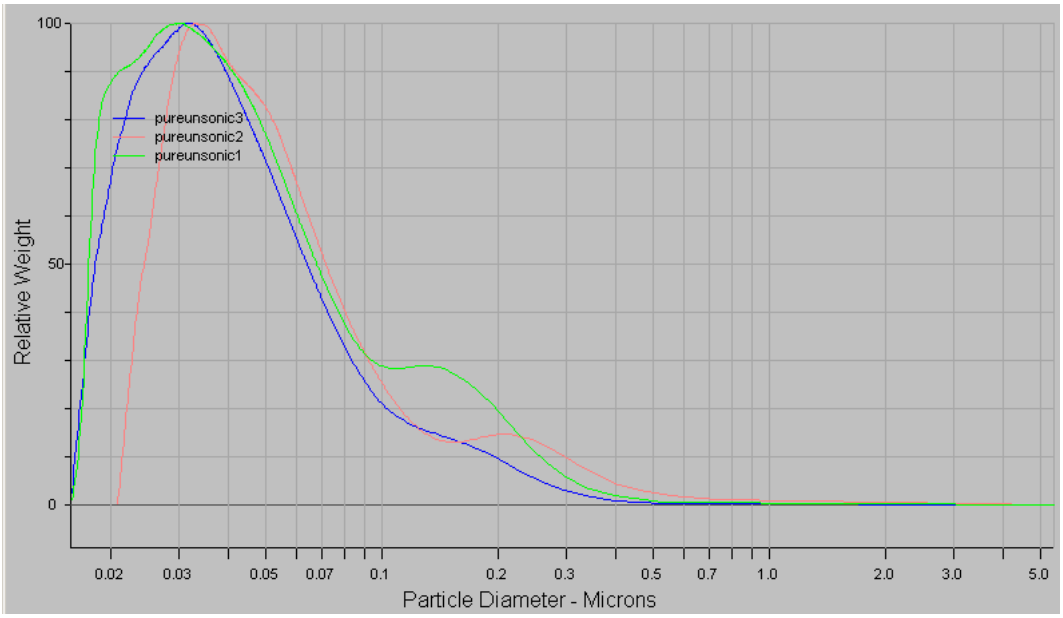

Figure 10 Size distribution of uncoated solid silica nanoparticles, not sonicated (old ratio substrate volumes, batch 1) measured by disc centrifuge. The sample was measured three times and each measurement is shown as different line colour. The x-axis corresponds to particle diameter in µm, whereas y-axis corresponds to relative weight of silica nanoparticles. Rotational speed of the disc centrifuge was 24,000 rpm.

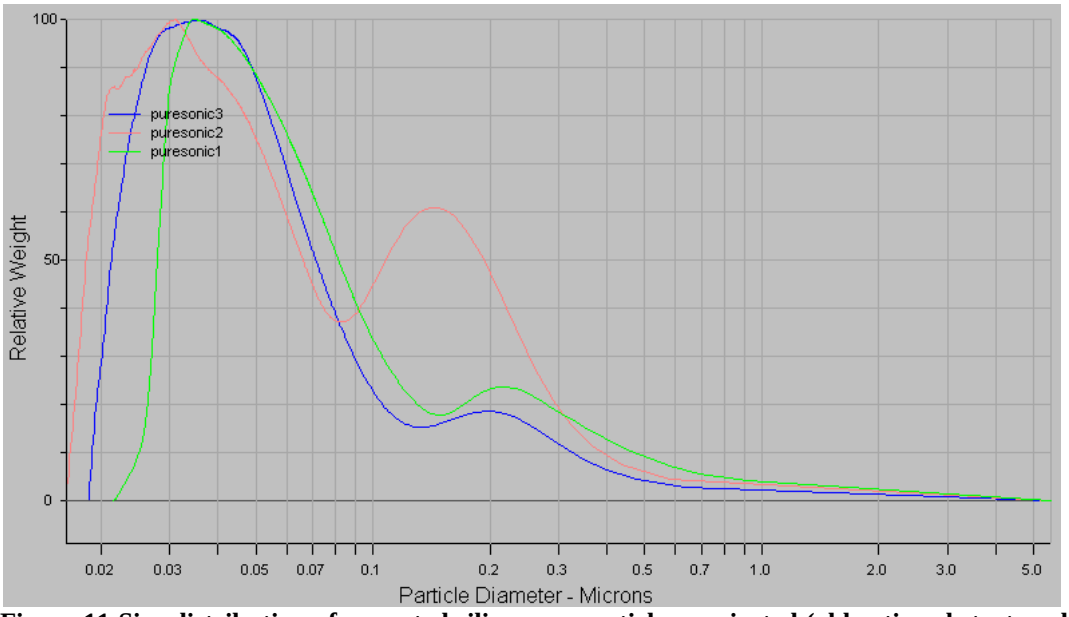

Figure 11 Size distribution of uncoated silica nanoparticles, sonicated (old ratio substrate volumes, batch 1) measured by disc centrifuge. The sample was measured three times and each measurement is shown as different line colour. The x-axis corresponds to particle diameter in µm, whereas y-axis corresponds to relative weight of silica nanoparticles. Rotational speed of the disc centrifuge was 24,000 rpm.

Figures 12 and 13 show clearly the change in size of nanoparticles with rotational speed alteration. Figure 13 indicated that more larger particles were present in the sample when rotational speed was reduced from 24,000 rpm to 12,000 rpm. Presence of a higher number of smaller particles (Figure 12) during application of 24,000 rpm may be explained by the fragile structure of the new ratio nanoparticles. As indicated by the SEM images (Table 2), these entities were fragmented in many cases. Also, nanoparticles were hollow what explained their susceptibility to breakage. Hence, high rotational speed may have caused damage to the structure so as to produce smaller fragments.

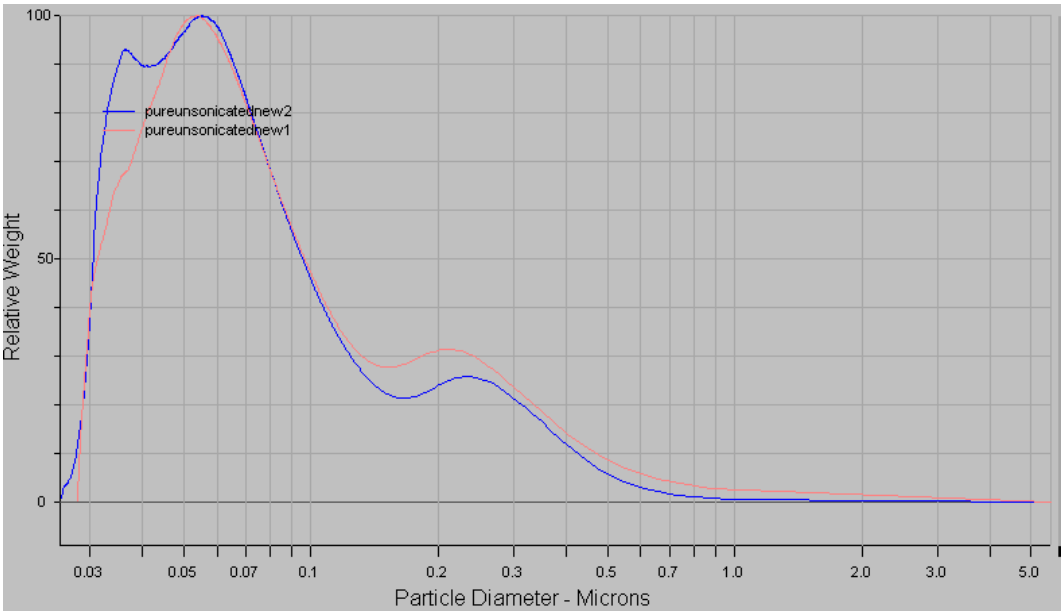

Figure 12 Size distribution of uncoated silica nanoparticles (new ratio substrate volumes) measured by disc centrifuge at 24,000 rpm. The sample was measured two times and each measurement is shown as different line colour. The x-axis corresponds to particle diameter in µm, whereas y-axis corresponds to relative weight of silica nanoparticles. Rotational speed of the disc centrifuge was 24,000 rpm.

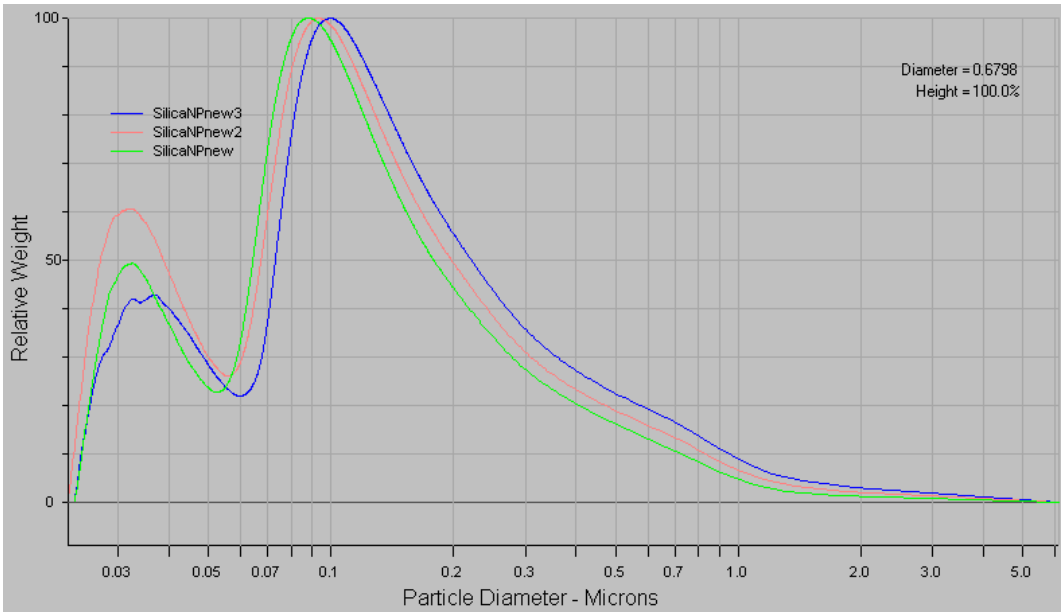

Figure 13 Size distribution of uncoated solid silica nanoparticles (new ratio substrate volumes) measured by disc centrifuge at 12,000 rpm. The sample was measured three times and each measurement is shown as different line colour. The x-axis corresponds to particle diameter in µm, whereas y-axis corresponds to relative weight of silica nanoparticles. Rotational speed of the disc centrifuge was 12,000 rpm.

3.1.3 Characterisation of DNA Aptamer – Silica Nanoparticle Construct

A spectrophotometer analysis showed that signals from FITC were present in both solid (non-porous) and mesoporous (porous) silica nanoparticle samples (Figures 14 and 15). Solid silica nanoparticles synthesised in this project are presented in Table 2. Mesoporous silica nanoparticles were supplied by Dr Townley and are shown in Figure 3. Fluorescence intensity of the FITC fluorophore fell within the expected wavelength range around 525 nm. Therefore, the incorporation of FITC on both solid and mesoporous silica nanoparticles was successful.

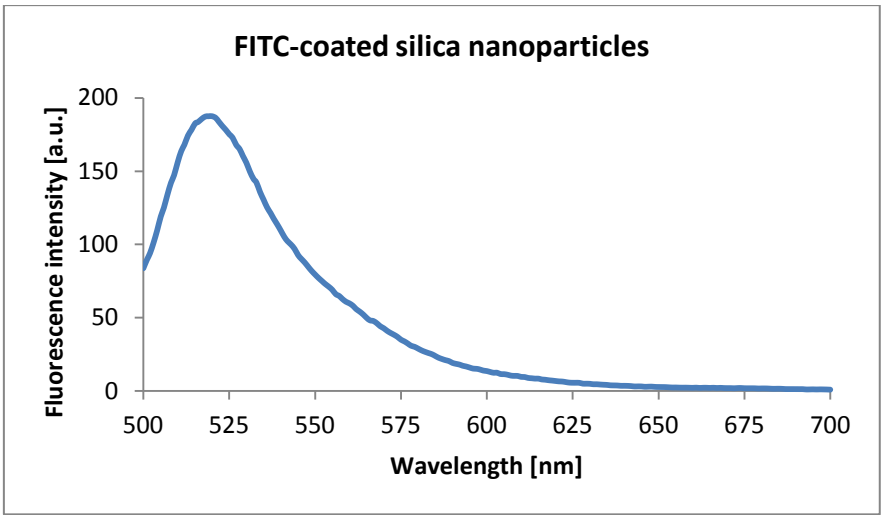

Figure 14 Fluorescence intensity of FITC fluorophores bound to the solid silica nanoparticles. The x-axis corresponds to wavelength in nm; the y-axis corresponds to fluorescence intensity in arbitrary units. The solid silica nanoparticles from batch 1 were used for this experiment.

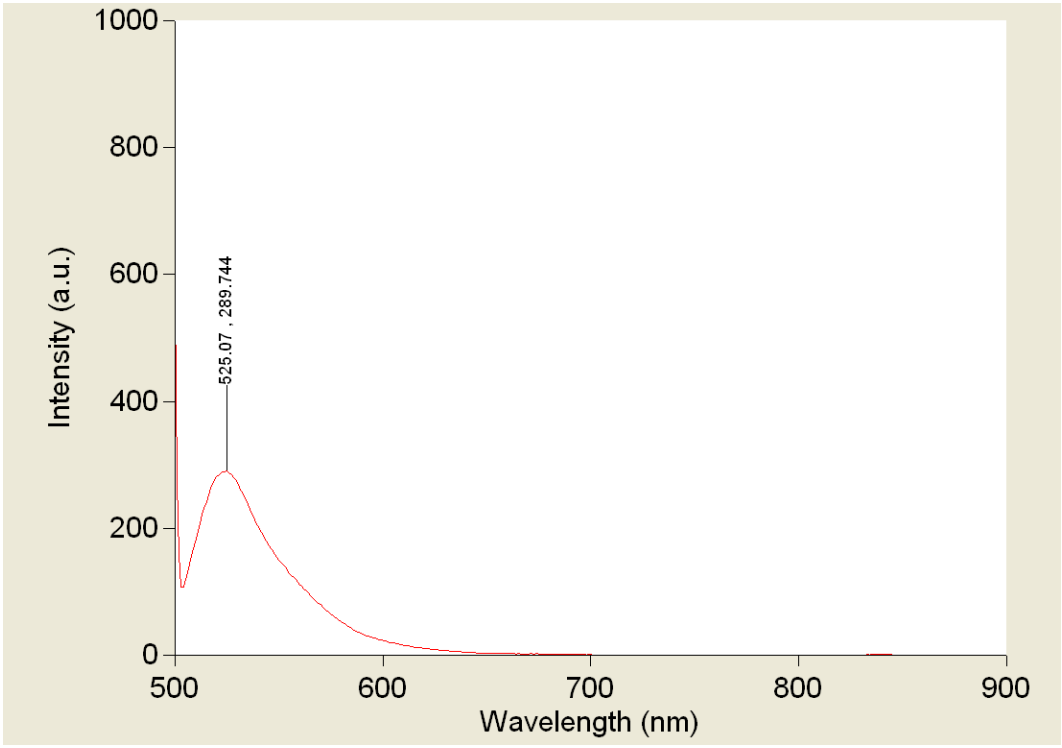

Figure 15 Fluorescence intensity of FITC fluorophore bound to modified mesoporous silica nanoparticles measured by fluorescence spectrophotometer. The x-axis corresponds to wavelength in nm, whereas y-axis corresponds to fluorescence intensity in arbitrary units. The mesoporous silica nanoparticles (provided by Dr Townley) were used in this experiment.

The disc centrifuge experiments of FITC-coated batch 1 silica nanoparticles (see Figures 16 and 17) showed that particle diameters of the coated particles were

comparable to the uncoated entities. Also, both sonicated and unsonicated FITC-coated particles were tested on the disc centrifuge and the results demonstrated presence of two peaks: 30-70 nm and 150-300 nm. Similarly to uncoated silica nanoparticles, a rotational speed of 24,000 rpm may have contributed to disruption of larger nanoparticle agglomerates. Hence, sonication did not have any additional disruption effects on the particles. However, it is crucial to observe that the sonicated sample gave still a 150-300 nm peak. This may suggest that the 150-300 nm peak does not belong to agglomerations but to monodisperse silica nanoparticles which are 150-300 nm in diameter. However the 150-300 peak may be an artifact caused by contamination from a disc centrifuge calibration standard solution or it can result from too short sonication time. No definite conclusion could be reached on the origin of the 150-300 nm peak. However, as we used only the mesoporous particles in fabrication of the full construct, this point was not pursued.

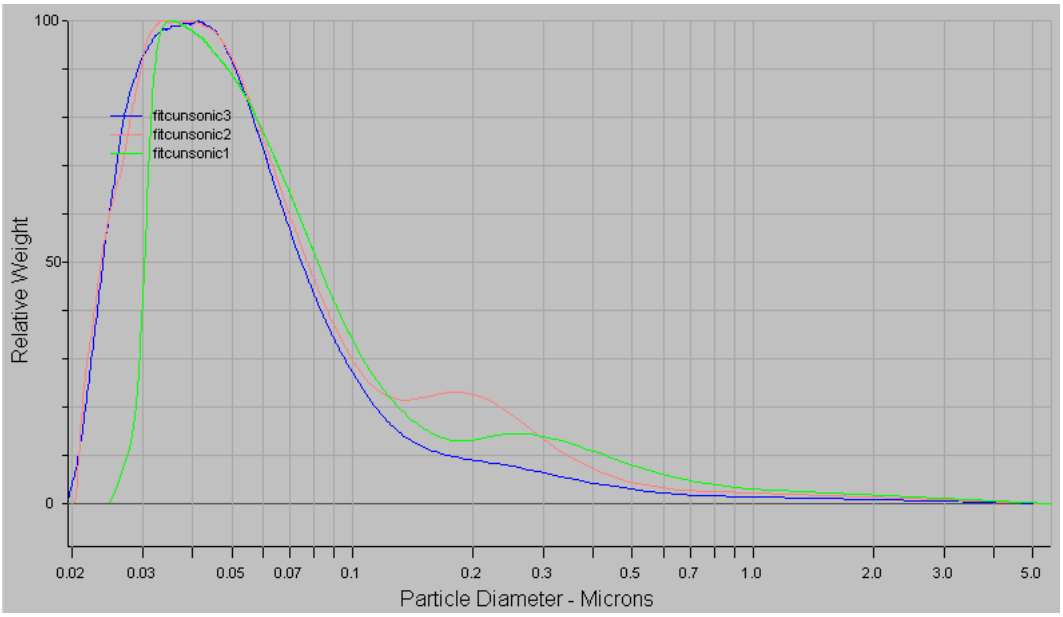

Figure 16 Size distribution of FITC-coated solid silica nanoparticles, not sonicated (old ratio substrate volumes, batch 1). The sample was measured three times and each measurement is shown as different line colour (red, green, blue). The x-axis corresponds to particle diameter in µm, whereas y-axis corresponds to relative weight of silica nanoparticles. Speed of a disc centrifuge was 24,000 rpm.

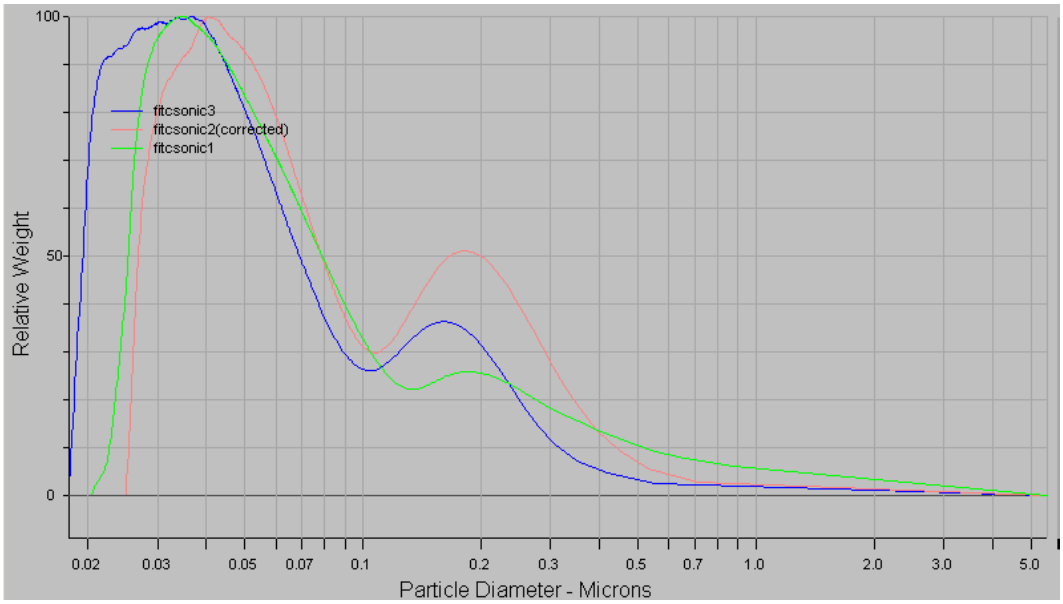

Figure 17 Size distribution of FITC-coated solid silica nanoparticles, sonicated (old ratio substrate volumes, batch 1). The sample was measured three times and each measurement is shown as different line colour (red, green, blue). The x-axis corresponds to particle diameter in µm, whereas y-axis corresponds to relative weight of silica nanoparticles. Speed of a disc centrifuge was 24,000 rpm.

A spectrophotometer study of aptamer-functionalised solid silica nanoparticles showed that weak signal from ATTO647N fluorophore was present in the investigated sample. The ATTO647N fluorophore (attached to the 5' end of the aptamer nucleotide sequence) gave the fluorescence intensity outcome at 660-670 nm wavelength (Figure 18) as anticipated. This signal indicated successful binding of aptamers to the silica nanoparticles. However, the fluorescence intensity from ATTO647N was not strong which may suggest a low level of attachment between silica nanoparticles and aptamers.

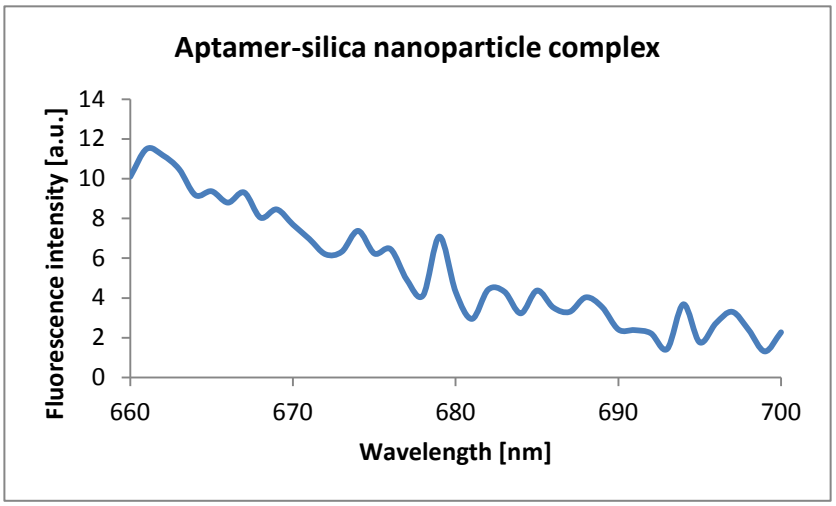

Figure 18 Fluorescence intensity of ATTO647N fluorophores bound to aptamer-silica nanoparticle complex. The x-axis corresponds to wavelength in nm, whereas y-axis corresponds to fluorescence intensity in arbitrary units. Solid silica nanoparticles from batch 1 synthesis were used in this experiment.

3.2 Synthesis of Superparamagnetic Construct and Magnetic Separation

3.2.1 Hybridisation and yield calculations.

In order to hybridise two DNA strands and form a hybrogen-bound double-helix, the melting temperature, T_m, was calculated. T_m is crucial for establishing successful DNA double-helix because above this temperature the DNA double-stand disassembles.

The formula for calculating melting temperature of DNA double-stand (Bartlett, 2002) is as follows:

$$T_m = 81.5 + 16.6 \times \log_{10}([Na^+]) + 0.41 \times (\%G + \%C) - (675/N)$$

Where

N – oligonucleotide fragment sequence, number of base pairs

%G – percentage of nucleotide guanine in an oligonucleotide fragment sequence

%C – percentage of nucleotide cytosine in an oligonucleotide fragment sequence

$[Na^+]$ – molar salt concentration

For the solutions used in these experiments:

$[Na^+]$ = 0.99%,

%G = %C = 38,

N = 21

T_m = 64.9°C

The hybridisation temperature should thus be kept below 64.9°C in order not to detach the two strands. In this way, the oligonucleotide fragment (which was attached to superparamagnetic nanoparticle) could be hybridised to aptamer and pull the complete construct from the solution.

Yields [%] of full aptamer separation after application of magnetic field were calculated from the following equation:

$$\text{Yield [\%]} = \frac{aptamer\ mass\ in\ the\ final\ pellet}{aptamer\ mass\ in\ the\ post\ hybridisation\ solution} \times 100\% \quad (1)$$

Mass of aptamers in the final pellet was calculated from the following equation:

$$\text{Mass [g]} = c \times V \times M \quad (2)$$

where:

c – aptamer concentration in the final pellet [mol l^{-1}]

V – volume of solution in which final aptamer pellet was dissolved [l]

M – aptamer molecular mass [g mol^{-1}]

Molecular mass of aptamers (*M*) was indicated by the supplier and was equal to:

$M_{aptamer}$ = 22656.9 g mol^{-1}

Equation (2) was also used for calculation of the mass of aptamers in the post hybridisation solution.

3.2.2. Hybridisation and separation of aptamer – oligonucleotide complex.

After selection of hybridisation temperature, aptamers, oligonucleotides and magnetic particles were mixed together in the Eppendorf tubes, so that the binding between aptamers and oligonucleotides as well as between oligonucleotides and superparamagnetic beads could occur at the same time. The volume of solution was 150 µl and after completion of each hybridisation this sample was taken for analysis on the plate reader and then returned to the Eppendorf tube for magnetic capture. The molar concentrations of aptamers during various stages this process are summed up in the Table 4. These molar concentrations were calculated from fluorescence intensities measured by the plate reader. The plate reader could measure the volume of 100 µl. The measured fluorescence intensities have thus been multiplied by a factor 1.5 in order to give a value for the 150 µl sample, except for the final pellet.

Table 4 Molar concentrations [nM] of aptamers at various stages of hybridisation and purification. The oligonucleotide fragments were added to the hybridisation solution to the final concentrations of 0 nM, 6.7 nM, 67 nM and 667 nM in four separate Eppendorf tubes. Aptamers were added to the hybridisation solution to the final concentration of 67 nM in each Eppendorf tube. The first column on the left corresponds to different stages during magnetic capture-hybridisation and corresponding molar concentrations of samples are provided in the subsequent columns. Aptamer concentrations in each sample were calculated from fluorescence intensity data measured by plate reader. The plate reader gain was 2900.

Molar concentrations of aptamers [nM]

Sample name	Final oligonucleotide concentration in solution [nM]			
	0	6.7	67	667
Post hybridisation (before separation)	66.5	62.9	59.4	67.2
Post hybridisation (after separation)	48.8	45.8	31.8	43.9
Wash 1	2.6	2.8	2.5	3.4
Wash 2	1.8	1.4	1.6	2.1
Wash 3	0.8	0.9	0.9	1.1
Wash 4	1.7	0.8	4.1	1.5
Pellet	0.3	4.0	10.8	0.7

Table 5 shows similar results to Table 4, but with an aptamer concentration increased from 67 nM to 100 nM and a greater addition of oligonucleotide fragments. Again the sample readings have been corrected for sample size.

Care had to be taken with the gain of the plate reader when measuring high values of the fluorescence (compare Table 5 and Table 6). The measured value for the pellet in experiment 3 in the Table 5 (denoted with N/A) must be an error, since it gave a higher value then that for the sample before separation. Therefore, this result was disregarded.

Table 5 Molar concentrations [nM] of aptamers at various stages of hybridisation and purification. The oligonucleotide fragments were added to the hybridisation solution to the final concentrations of 0 nM, 67 nM, 667 nM and 6667 nM in four separate Eppendorf tubes. Aptamers were added to the hybridisation solution to the final concentration of 100 nM in each Eppendorf tube. The first column on the left corresponds to different stages during magnetic capture-hybridisation and corresponding molar concentrations of samples are provided in the subsequent columns. Aptamer concentrations in each sample were calculated from fluorescence intensity data measured by plate reader. The plate reader gain was 2900.

Molar concentration of aptamers [nM]

Sample name	Final oligonucleotide concentration in solution [nM]			
	0	67	667	6667
Post hybridisation (before separation)	67.0	92.4	90.1	98.4
Post hybridisation (after separation)	48.9	53.9	29.0	70.5
Wash 1	4.0	3.7	2.4	6.2
Wash 2	2.0	2.0	2.4	1.2
Wash 3	1.4	1.1	2.2	1.1
Wash 4	1.3	5.0	20.5	1.2
Pellet	0.4	18.3	N/A	6.2

Table 6 Molar concentrations [nM] of aptamers at various stages of hybridisation and purification. The oligonucleotide fragments were added to the hybridisation solution to the final concentrations of 0 nM, 67 nM, 667 nM and 6667 nM in four separate Eppendorf tubes. Aptamers were added to the hybridisation solution to the final concentration of 100 nM in each Eppendorf tube. The first column on the left corresponds to different stages during magnetic capture-hybridisation and corresponding molar concentrations of samples are provided in the subsequent columns. Aptamer concentrations in each sample were calculated from fluorescence intensity data measured by plate reader. The plate reader gain was 2800.

Molar concentrations of aptamers [nM]				
Sample name	Final oligonucleotide concentration in solution [nM]			
	0	67	667	6667
Post hybridisation (before separation)	68.5	90.6	85.2	97.8
Post hybridisation (after separation)	49.4	51.7	28.7	74.2
Wash 1	4.2	4.5	2.8	5.6
Wash 2	1.8	2.2	2.7	2.2
Wash 3	1.5	1.3	2.0	1.6
Wash 4	1.6	4.3	20.9	2.1
Pellet	0.2	14.9	N/A	5.3

The fluorescence intensity measurements enabled calculation of aptamer concentrations from the calibration curves (different for each plate reader gain) presented in the Appendix. After the concentrations were obtained, the corresponding masses and yields could be calculated (the equations for these calculations were given in section 4.2.1).

Table 7 shows the concentrations calculated from the calibration curves (see Appendix) for gains 2900 and 2800. Table 8 shows the aptamer masses and yields calculated from concentrations.

Table 7 Molar concentrations [nM] of aptamers in post hybridisation solution sample and final pellet sample.

Concentration of aptamers in the solution [nM]	Concentration of oligonucleotide in the solution [nM]	Concentration of aptamer in post hybridisation solution [nM]	Concentration of aptamer in final pellet [nM]	Gain
67	667	67.2	0.7	2900
67	67	59.4	10.8	2900
67	6.7	62.9	4.0	2900
100	6667	97.8	5.3	2800
100	667	85.2	N/A	2800
100	67	90.6	14.9	2800

Table 7 shows that the oligonucleotide concentration which gave the best binding to aptamers was 67 nM for aptamer concentrations of 67 and 100 nM. Oligonucleotide concentrations of 667 nM or 6667 nM did not increase the amount of aptamers in the final pellet.

Table 8 is a summary of mass and yield calculations. The yields for these magnetic capture-hybridizations were still low and variable. Thus it was decided to attempt a different binding scheme for a substantially complete construct, omitting only the silica nanoparticle. The components of this construct were bound at the same time, when aptamers, oligonucleotides and magnetic beads were added to the hybridisation buffer.

Table 8 Magnetic capture-hybridisation yields [%] of aptamers (various oligonucleotide fragment concentrations).

Concentration of aptamers in post hybridisation solution [nM]	Concentration of aptamers in the final pellet [nM]	Mass of aptamers in the post hybridisation solution [g]	Mass of aptamers in the final pellet [g]	Yield [%]
67.2	0.7	2.3×10^{-7}	2.4×10^{-9}	1.0
59.4	10.8	2.0×10^{-7}	3.7×10^{-8}	18.5
62.9	4.0	2.1×10^{-7}	1.4×10^{-8}	6.7
97.8	5.3	3.3×10^{-7}	1.8×10^{-8}	5.5
85.2	N/A	2.9×10^{-7}	N/A	N/A
90.6	14.9	3.1×10^{-7}	5.1×10^{-8}	16.5

3.2.3 Hybridisation and separation of aptamer – mesoporous silica nanoparticle construct

Due to variable yields obtained by the previous magnetic capture-hybridisation method (see Table 8) a new binding order was tried. Also, mesoporous silica nanoparticles (provided by Dr Townley) were included in construct fabrication experiments. Solid silica nanoparticles produced previously were not used in this investigation due to suspected agglomeration problems which could have limited a construct synthesis. As a first step, the mesoporous silica nanoparticles were functionalised with aptamers. The success of this binding was confirmed by fluorescence intensity measurement of ATTO647N fluorophores attached to aptamers. Second, oligonucleotide fragments were bound to magnetic particles. Finally, the full construct could be fabricated by hybridisation of aptamers with oligonucleotide fragments. As in the previous study the fluorescence intensities of magnetically captured constructs were measured and were adjusted to the used volumes accordingly.

Various amounts of oligonucleotide were added into the final hybridisation solution (Tables 9 - 11). 30 µl of mesoporous silica nanoparticle – aptamer complex were added to the first hybridisation solution (Table 9). The outcomes presented in Table 9 suggest that smaller concentration of oligonucleotide fragments in solution gives better hybridisation results when 30 µl of mesoporous silica nanoparticle – aptamer were added.

Table 9 Molar concentrations [nM] of aptamers at various stages of hybridisation and purification for 30 µl aptamer-functionalised mesoporous silica nanoparticle added to hybridisation solutions. The oligonucleotide fragments were added to the hybridisation solution to the final concentrations of 1100 nM, 110 nM and 11 nM in three separate Eppendorf tubes and to the final concentrations of 110 nM, 11 nM and 1 nM in next three Eppendorfs. Aptamers-mesoporous silica nanoparticle volumes of 30 µl were added to each Eppendorf. The first column on the left corresponds to different stages during magnetic capture-hybridisation and corresponding molar concentrations of samples are provided in the subsequent columns. Aptamer concentrations in each sample were calculated from fluorescence intensity data measured by plate reader. The plate reader gain was 3500.

Molar concentrations of aptamers [nM]						
Sample name	Oligonucleotide concentration in solution [nM]			Oligonucleotide concentration in solution [nM]		
	1100	110	11	110	11	1
	30 µl mesoporous silica particle – aptamer solution					
Post hybridisation (before separation)	214.6	229.6	163.7	216.9	196.0	177.4
Post hybridisation (after separation)	154.4	157.8	160.5	129.3	169.6	184.4
Wash 1	5.0	4.0	3.0	0.7	2.8	1.8
Wash 2	1.7	1.4	0.6	1.7	1.7	0.5
Wash 3	0.7	0.7	0.5	2.1	0.2	2.7
Wash 4	2.7	2.1	0.7	4.6	1.9	2.3
Pellet	15.7	3.0	N/A	22.3	2.9	N/A

Due to low binding obtained by addition of 30 µl of mesoporous silica nanoparticle – aptamer complex to the hybridisation solution, the mesoporous silica nanoparticle – aptamer complex volume was increased to 50 µl (Table 10). The increase in aptamer

concentration in the solution did not result in the formation of more of the full construct. Compare results for similar conditions in Table 9 and Table 10.

The data presented in Table 10 show some similarity to data from Table 9. The lower oligonucleotide concentrations resulted in better aptamer binding represented by somewhat higher concentrations of aptamer present in the final pellet.

Table 10 Molar concentrations [nM] of aptamers at various stages of hybridisation and purification for 50 µl aptamer-functionalised mesoporous silica nanoparticle added to hybridisation solution. The oligonucleotide fragments were added to the hybridisation solution to the final concentrations of 1100 nM, 110 nM and 11 nM in three separate Eppendorf tubes and to the final concentrations of 110 nM, 11 nM and 1 nM in next three Eppendorfs. Aptamers-mesoporous silica nanoparticle volumes of 50 µl were added to each Eppendorf. The first column on the left corresponds to different stages during magnetic capture-hybridisation and corresponding molar concentrations of samples are provided in the subsequent columns. Aptamer concentrations in each sample were calculated from fluorescence intensity data measured by plate reader. The plate reader gain was 3500.

Molar concentrations of aptamers [nM]						
Sample name	Final oligonucleotide concentration in solution [nM]			Final oligonucleotide concentration in solution [nM]		
	1100	110	11	110	11	1
	50 µl mesoporous silica particle – aptamer					
Post hybridisation (before separation)	408.6	479.4	463.5	423.4	406.7	427.6
Post hybridisation (after separation)	386.0	396.7	343.9	285.6	250.1	343.5
Wash 1	4.1	2.6	3.0	6.4	3.6	5.5
Wash 2	1.2	1.7	2.6	3.2	1.0	1.4
Wash 3	1.4	N/A	0.1	2.2	1.4	1.0
Wash 4	6.7	1.2	1.1	4.8	1.3	1.7
Pellet	0.9	0.2	0.1	31.6	3.8	N/A

Finally, various aptamer volumes (30, 10 and 5 µl) were added to the final hybridisation solutions (Table 11). Similarly to the previous outcomes, lower oligonucleotide concentrations in the solution resulted in better aptamer binding and higher concentrations of aptamers present in the final pellet.

On the other hand, higher oligonucleotide concentrations (1100 – 11 nM range) gave outcomes similar to those in Table 10, where aptamer binding to nucleotide was within the error limit.

Table 11 Molar concentrations [nM] of aptamers at various stages of hybridisation and purification for various volumes of aptamer-functionalised mesoporous silica nanoparticle added to hybridisation solutions. The oligonucleotide fragments were added to the hybridisation solution to the final concentrations of 1100 nM in three separate Eppendorf tubes and to the final concentrations of 110 nM in next three Eppendorfs. Aptamers-mesoporous silica nanoparticle volumes of 30 µl 10 µl and 5 µl were added to Eppendorfs as indicated. The first column on the left corresponds to different stages during magnetic capture-hybridisation and corresponding molar concentrations of samples are provided in the subsequent columns. Aptamer concentrations in each sample were calculated from fluorescence intensity data measured by plate reader. The plate reader gain was 3500.

Molar concentrations of aptamers [nM]						
Sample name	1110 nM oligonucleotide concentration in solution			110 nM oligonucleotide concentration in solution		
	Mesoporous silica particle – aptamer volume [µl]					
	30	10	5	30	10	5
Post hybridisation (before separation)	257.4	79.9	47.0	233.4	69.3	49.3
Post hybridisation (after separation)	252.2	65.4	41.3	159.6	60.5	42.7
Wash 1	3.4	1.2	1.6	3.7	2.0	1.6
Wash 2	1.7	1.5	0.9	2.5	1.2	1.6
Wash 3	0.6	2.4	1.2	0.8	1.3	0.7
Wash 4	2.1	0.2	0.1	2.3	1.3	0.5
Pellet	N/A	N/A	N/A	13.0	3.6	2.1

Table 12 summarises the concentrations of aptamers in the post hybridisation solution and in the final pellet. In can be observed that higher oligonucleotide concentrations do not result in better aptamer binding. Increasing or decreasing aptamer concentration does not seem to remedy the low binding to oligonucleotides.

Table 12 Molar concentrations [nM] of aptamers in post hybridisation solution samples and final pellet samples.

Volume of aptamer-mesoporous silica added [μl]	Concentration of oligonucleotides in the solution [nM]	Concentration of aptamer in post hybridisation (before separation) solution [nM]	Concentration of aptamer in the final pellet [nM]
30	1100	214.6	15.7
30	110	229.6	3.0
30	11	163.7	N/A
50	1100	408.6	0.9
50	110	479.4	0.2
50	11	463.5	0.1
30	1100	257.4	N/A
10	1100	79.9	N/A
5	1100	47.0	N/A

Table 13 Magnetic capture-hybridisation yield [%] of aptamer-functionalised mesoporous silica nanoparticles (high oligonucleotide fragment concentration).

Concentration of aptamers in the post hybridisation solution [nM]	Concentration of aptamers in the final pellet [nM]	Mass of aptamers in the post hybridisation solution [g]	Mass of aptamers in the final pellet [g]	Yield [%]
214.6	15.7	1.46×10^{-6}	3.63×10^{-8}	2.5
229.6	3.0	1.56×10^{-6}	6.80×10^{-9}	0.4
163.7	N/A	1.11×10^{-6}	N/A	N/A
408.6	0.9	2.78×10^{-6}	2.04×10^{-9}	0.1
479.4	0.2	3.26×10^{-6}	4.53×10^{-10}	Negligible
463.5	0.1	3.15×10^{-6}	2.27×10^{-10}	Negligible
257.4	N/A	1.75×10^{-6}	N/A	N/A
79.9	N/A	5.44×10^{-7}	N/A	N/A
47.0	N/A	3.19×10^{-7}	N/A	N/A

Table 14 shows results of aptamer hybridisation to oligonucleotide fragments when concentration of oligonucleotide stock solution was diluted ten times. In comparison to

Table 12, there is significant improvement over aptamer-oligonucleotide binding. It should be noticed that oligonucleotide concentration of 1 nM only did not show any aptamer-oligonucleotide hybridisation.

Table 14 Molar concentrations [nM] of aptamers in post hybridisation solution samples and final pellet samples.

Volume of aptamer-mesoporous silica added [µl]	Concentration of oligonucleotide in the solution [nM]	Concentration of aptamers in post hybridisation (before separation) solution [nM]	Concentration of aptamer in the final pellet [nM]
30	110	216.9	22.3
30	11	196.0	2.9
30	1	177.4	N/A
50	110	423.4	31.6
50	11	406.7	3.8
50	1	427.6	N/A
30	110	233.4	13.0
10	110	69.3	3.6
5	110	49.3	2.1

Table 15 shows yields of full construct formation and although the yields are low (0.3 – 3.4%), these outcomes are higher than those calculated in Table 13. However, the yields from Table 15 are not as high as results from aptamer-oligonucleotide-magnetic particle complex formation (Table 8).

Table 15 Magnetic capture-hybridisation yield [%] of aptamer-functionalised mesoporous silica nanoparticles (low oligonucleotide fragment concentration).

Concentration of aptamers in post hybridisation solution [nM]	Concentration of aptamers in the final pellet [nM]	Mass of aptamers in the post hybridisation solution [g]	Mass of aptamers in the final pellet [g]	Yield [%]
216.9	22.3	1.47×10^{-6}	4.98×10^{-8}	3.4
196.0	2.9	1.33×10^{-6}	6.80×10^{-9}	0.5
177.4	N/A	1.20×10^{-6}	N/A	N/A
423.4	31.6	2.88×10^{-6}	7.25×10^{-8}	2.5
406.7	3.8	2.77×10^{-6}	9.06×10^{-9}	0.3
427.6	N/A	2.91×10^{-6}	N/A	N/A
233.4	13.0	1.58×10^{-6}	2.95×10^{-8}	1.9
69.3	3.6	4.69×10^{-7}	9.06×10^{-9}	1.9
49.3	2.1	3.33×10^{-7}	4.53×10^{-9}	1.4

In summary, the highest yields calculated for purification of the aptamers (no silica nanoparticles) by magnetic capture-hybridisation were 18.5% and 16.5% (Table 8). These yields were achieved when difference between concentrations of the aptamers and the oligonucleotides in solution was the smallest.

When aptamer-functionalised mesoporous silica nanoparticles were isolated by magnetic field, higher yields were reached when oligonuleotide concentrations in hybridisation solution ranged between 1 – 110 nM rather than 11- 1100 nM.

3.3 MUC-1 Biomarker Detection

3.3.1 Detection of MUC-1 biomarker with monoclonal antibody

Figure 19 shows that the blue nuclear dye (DAPI) stained cell nuclei. It penetrated the membranes of MCF7 cells and, in this way, confirmed that the breast cancer cells were present in the analysed samples.

During immunohistochemistry experiments a primary antibody was introduced to MCF7 samples and attached specifically to mucin-1 biomarkers. The success of this binding was proven by attachment of the FITC-linked secondary antibody which was specific to the primary antibody. The FITC fluorophore was excited by the laser beam and emitted a 520 nm spectrum which was visualised by the fluorescent microscope and was visible as a green colour (Figure 19). The results indicated that mucin-1 biomarkers are present on MCF7 cells. However, only minute binding between antibodies and cells occurred. This may be attributed to low antibody concentration introduced during immunohistochemistry or too short incubation time.

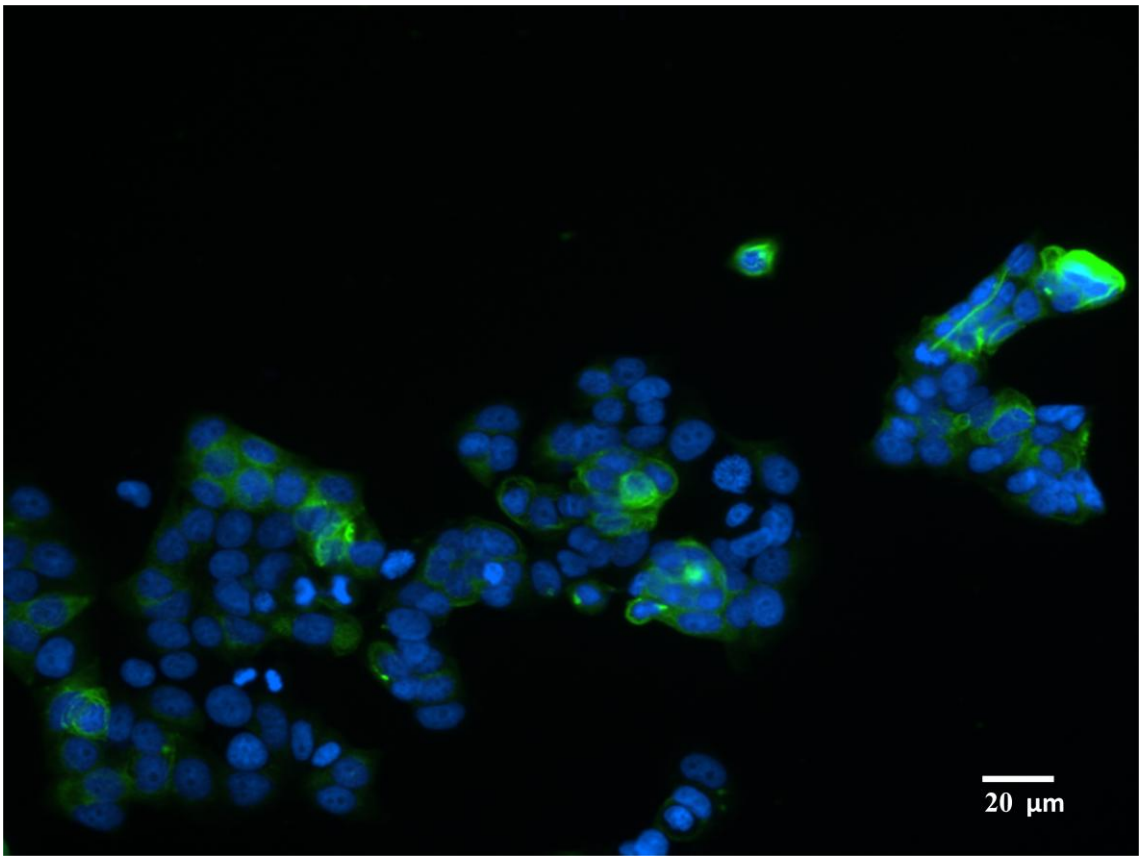

Figure 19 Fluorescence microscopy image of MUC-1 expressing MCF7 cells. Anti-MUC-1 primary antibodies bound to MUC-1 expressed on the surface of MCF7 cells. FITC-bound secondary antibodies attached to primary antibodies (shown in green), thus indicating presence of MUC-1 on the surfaces of MCF7 cells. MCF7 cells nuclei were labelled with DAPI nuclear dye (shown in blue).

3.3.2 DNA aptamer binding to MUC-1 biomarker

Flow cytometry (FACS) analysis was conducted in order to determine whether DNA aptamers are able to bind MCF7 metastatic breast cancer cells. The aptamers had fluorophores ATTO647N bound to them. Upon successful binding between DNA aptamers and MCF7 cells, we then expected the signal from fluorophore to be detected by flow cytometer.

The flow cytometry study involved examination of the three sets of samples: MCF7 cells without aptamer labelling incubated at 4°C, MCF7 cells incubated with aptamers at 37°C for 30 minutes and MCF7 cells incubated at 4°C for 1.5 hour.

Figure 20 indicates a population of cells which was recognized as suitable for analysis and labelled as population one (P1). The group of cells marked as red dots represent

whole and live entities as opposed to black dots which were identified as cell debris. Figure 20 enables differentiation between various cells by analysis of a side scatter (SSC-A) on y-axis and a forward scatter (FSC-A) on x-axis. The side scatter generated during flow cytometry measurements reflects cellular granularity and the forward scatter measures relative cell size. Hence, only cells of large enough size and granularity are identified as live thus suitable for fluorescence examination.

Figure 21 shows MFI P2 population of cells. This area is dedicated to cells which display bound ATTO647N fluorophore and are therefore fluorescent. However, in this case the MFI P2 population shows that only 1.1% of cells are fluorescent. This is an inherent fluorescence of MCF7 cells and can be disregarded. It is also in agreement with expected results as the ATTO647N fluorophore was not present in this sample.

Similarly to flow cytometry data for unlabelled MCF7 cells, the fluorescence was measured for cells bound to aptamers. The aptamers were mixed with the MCF7 cells in various concentrations. These MCF7 cells were grown immobilized on a plastic container when aptamers were loaded on their surface. One sample however was treated differently: the cells in solution were added to an Eppendorf, and the aptamer was added and left to incubate. For both the immobilised cells and the cells in solution, two incubation temperatures were tested, as shown in Table 16. The results of this study showed varying results (see Tables 16 and 17). Table 16 indicates that better aptamer binding to MCF7 cells was achieved when cancer cells were suspended in solution. Within the initial population 35.8% and 44% of cells were fluorescent, thus they bound to aptamers. As for immobilised cells, better aptamer binding was attained for 37°C incubation temperatures than for 4°C incubation. However, Table 17 shows that immobilised MCF7 cells were binding aptamers better. Moreover, overall binding to MCF7 cells increased by a few percent. The discrepancy in these results may be due to

problems with resuspension of immobilised cells for FACS sample preparation as well as too high concentrations of cells taken for analysis.

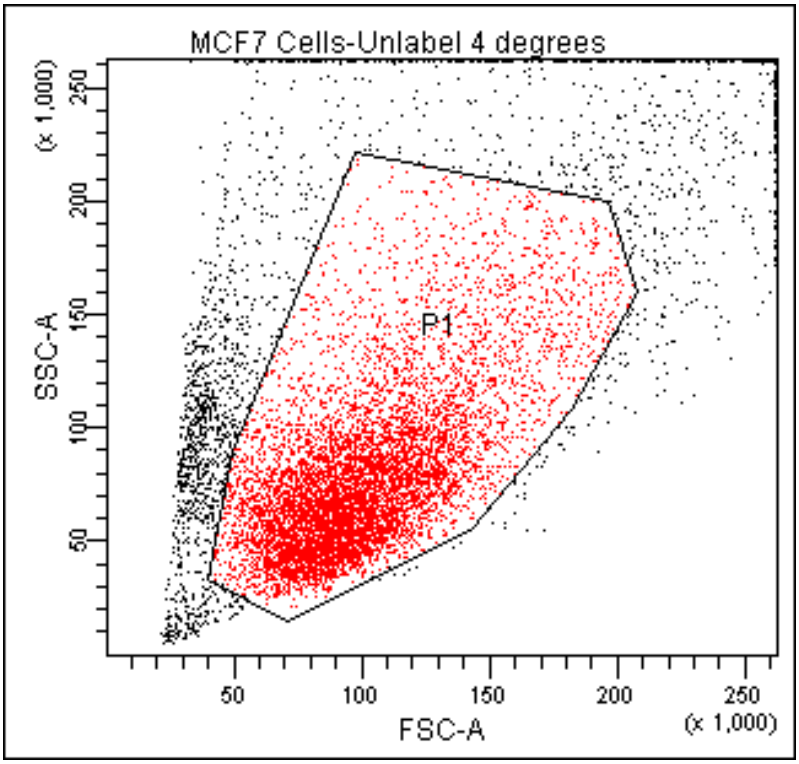

Figure 20 FACS image of unlabelled MCF7 cell population incubated at 4°C.

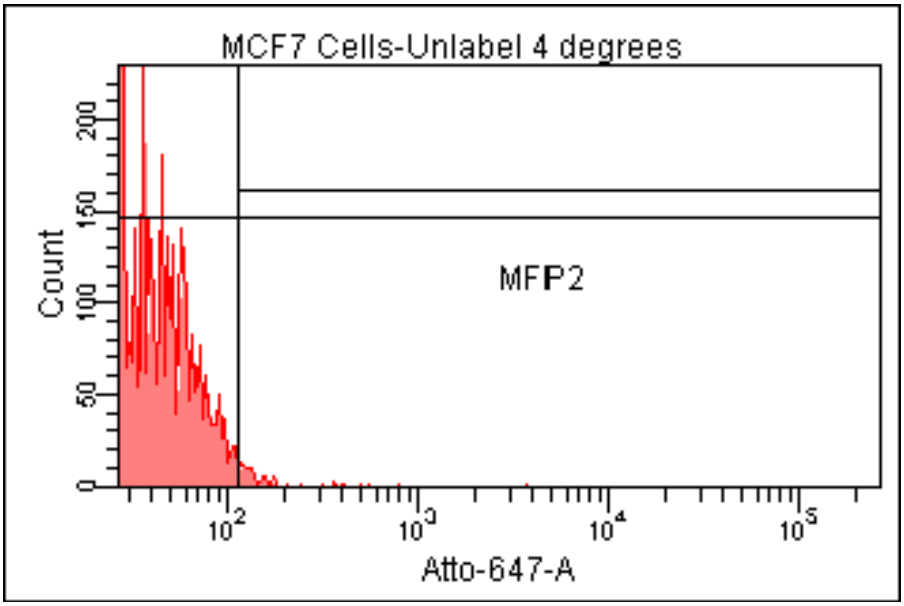

Figure 21 Unlabelled MCF7 cells incubated at 4°C indicating cell number versus cell fluorescence.

Table 16 FACS measurements of MCF7 cells bound to aptamers.

Aptamer concentration [nM]	Cells bound to aptamers [%]	
	Incubation temperature 4ºC	Incubation temperature 37ºC
100 (in solution)	35.8	44.0
100	1.7	15.9
10	1.8	3.6
1	1.7	2.6

Table 17 FACS measurements of MCF7 and CHO cells bound to aptamers.

Aptamer concentration [nM]	Cells bound to aptamers [%] at 4°C	
	MCF7 cells	CHO cells
100 (in solution)	9.2	7.4
100	32.8	21.5
10	6.3	6.6

4 Discussion and Conclusions

This proof-of-concept study describes a method of making and purifying silica nanoparticles with aptamer-functionalised surfaces. These constructs may be applied in cancer diagnosis and therapy. The method used for isolation of the constructs was magnetic capture-hybridisation (Hornes and Korsens, 1990).

The solid silica nanoparticles were synthesised by a modified Stöber method with the objective of producing 60 nm monodisperse particles. However, despite using the same concentrations of TEOS, water and ammonium ions as recommended by Rao *et al.* (2005), the desired 60 nm particle diameter could not be reliably attained. According to SEM images of the nanoparticles their diameter varied between 116 and 215 nm. The difficulties with obtaining the desired nanoparticle size were ascribed to the sensitivity of the Stöber method. The Stöber synthesis depends on temperature, method and time of substrate addition. If any of these parameters is changed the outcome varies, and is thus sensitive to experimental technique as discussed by Park *et al*., (2002).

The sizes of solid silica nanoparticles were determined by several methods: disc centrifuge, Zetasizer, NanoSight and SEM. Several discrepancies between outcomes from these devices were observed. The SEM images provided the most reliable method of size determination as the synthesised nanoparticles could be directly observed on the images. NanoSight analysis indicated nanoparticle sizes similar to those identified by SEM. However, results obtained from disc centrifuge and Zetasizer differed from SEM and NanoSight. In the case of the disc centrifuge operational software provided a plot of relative weight of nanoparticles against their diameters. The relationship between numbers of silica nanoparticles and their diameter sizes was not given, so interpretation of these plots was not clear.

In order to investigate the existence of attractive interactions between nanoparticles which could affect the size measurement, the zeta potential of the nanoparticles was determined. This study revealed that at pH 5-8 the solid silica nanoparticles should have remained in a dispersed, non-agglomerated state. However, the possibility of attractive interactions between nanoparticles was not excluded and further experiments to detect possible agglomeration were performed. BSA was added as a first approach and the rotational speed change of the disc centrifuge was varied in a second trial. The addition of BSA proved to be inconclusive because it contaminated the samples. On the other hand, disc centrifuge measurements revealed that indeed there was an increase in the silica nanoparticle diameters when rotational speed was reduced. This result seemed to corroborate a hypothesis of agglomerate formation, though the outcome might also have resulted from nanoparticle breakage. The latter conclusion was supported by inspection of SEM images, which revealed the presence of many broken and hollow nanoparticles (Table 2). We concluded that the fragility of these silica nanoparticles made them prone to breakage and resulted in lower particle size at higher rotational speeds. Hence, neither disc centrifuge nor Zetasizer constitute reliable methods for these silica nanoparticle size investigations. Scanning electron microscopy should be used as the first approach for determination of the silica nanoparticle diameters.

The solid silica nanoparticles from batch 1 were successfully coated with FITC fluorophores. The fluorophore attachment was confirmed by fluorescence spectrophotometry which showed the emission spectrum in the expected range. The method of FITC binding thus worked well and could be used in future studies. The FITC-doped solid silica nanoparticles were functionalised with the ATTO647N fluorophore-labelled aptamers. However, fluorescence spectrophotometry showed very

little emission at 660 to 670 nm indicating that the aptamers were indeed conjugated to solid silica nanoparticles but that their quantity was low.

The magnetic capture-hybridisation was preceded by fabrication of two constructs. The first comprised aptamers bound to an oligonucleotide–magnetic particle complex by hydrogen bonds; the second consisted of mesoporous silica nanoparticles bound by aptamer-oligonucleotide fragments to superparamagnetic iron oxide core particles. The success of magnetic capture-hybridisations of both constructs was proved by measurement of fluorescence intensity of the ATTO647N fluorophore bound to the aptamer. Although, the magnetic capture-hybridisation was successful, the calculation of yields indicated that only a small fraction of aptamers or aptamer-functionalised mesoporous silica nanoparticles could be purified from solution by this method (0.1-3%). On the other hand, when a construct lacking the silica nanoparticles was synthesised, the yields of aptamer recovered with magnetic field from the solution reached as high as 18.5%. We conclude that the low yields of full construct synthesis may be attributed to the influence of silica nanoparticle binding. It is possible for the silica nanoparticles to bind many aptamers on their surfaces, so that the number of aptamers available for interaction with oligonucleotide fragments is lower. On the other hand, when silica nanoparticles are absent, the aptamers floating in solution are free to interact with oligonucleotides and form double-helices. Also, the low yields of magnetic purification overall could be ascribed to the complicated tertiary structure of aptamers which could have been an obstacle in forming a double strand hybrid with oligonucleotide fragments. This suggests that the method of magnetic capture-hybridisation, although successful, needs to be optimised in order to obtain higher purification yields. Moreover, it is noteworthy that the highest hybridisation yields were obtained when the difference between aptamer and oligonucleotide concentration in the

solution was the smallest. This may suggest an inhibitory effect on hybridisation if one of the binding partners (aptamers or oligonucleotides) is more abundant in the solution. Furthermore, the pore size of mesoporous silica nanoparticles might have been large enough to allow capture of aptamers inside the pores. This would reduce the aptamer concentration available in solution resulting in lower yields. In order to eliminate the possibility of aptamer entry into the nanoparticle pores it would be necessary to use solid silica nanoparticles instead of mesoporous silica. Moreover, if mesoporous silica nanoparticles were applied again, both pore diameters and aptamer sizes would need to be measured.

Aptamer-functionalised silica nanoparticles can be applied in detection of mucin-1 biomarkers present on the surface of MCF7 cells. They can also be used in the delivery of a therapeutic payload. They may thus prove to be important in the targeting of metastatic breast cancer cells, which pose a serious threat to human health. In order to achieve this, the aptamers must have a proven ability to bind MCF7 cells *in vitro* and should be successfully attached to the surface of monodisperse and uniformly-sized silica nanoparticles.

The presence of MUC-1 biomarkers on the surface of MCF7 metastatic breast cancer cells was confirmed by attachment of anti-mucin-1 antibodies. However, the images from fluorescence microscopy showed low binding to the cells. This may be a consequence of low concentration of antibodies, their insufficient affinity for mucin-1 biomarkers or the short incubation times used in these experiments.

The binding of aptamers to MCF7 cells was corroborated with flow cytometry (FACS). The results indicated that indeed the aptamers bind to MUC-1 (expressed by MCF7 cells) which is in agreement with Ferreira *et al*. (2009). However the optimum conditions for the binding could not be deduced from this study, perhaps because too

high a number of cells was used in these experiments, or due to problems with their detachment from the vessel surfaces. It is also possible that the aptamer concentration was too low. The protocol needed to achieve maximum aptamer binding to immobilised MCF7 should be further investigated.

5 Future Directions

The sizes and shapes of solid silica nanoparticles were measured by various instruments. The SEM results indicated distinctive batch-to-batch variation. Furthermore, some particles were aggregated and otherwise hollow. This may hinder efficient aptamer binding to the surface of particles and thus cause inefficient attachment to MUC-1 biomarkers. Also, the mesoporous silica nanoparticles obtained higher diameters than expected, although agglomeration was not observed. Addition of BSA did not help in breaking the nanoparticle complexes, therefore other method for agglomeration prevention must be established. Perhaps functionalisation of silica nanoparticle surface with PEG chains would offer a solution to this issue. In conclusion, based on the outcomes from the solid silica fabrication study, it will be necessary to establish a protocol which will provide monodisperse silica nanoparticles of reproducible size.

It is also suggested that the silica nanoparticles to be used in the following studies should be changed to mesoporous silica nanoparticles permanently. Mesoporous silica particles contain multiple pores which may carry therapeutic payloads. This sort of particle may be directed to the sites of disease by a specifically-binding ligand and eradicate the malfunctioning cells. Moreover, mesoporous silica nanoparticles have larger surface area because of the presence of pores, hence better aptamer binding might be attained.

Two constructs were successfully fabricated: aptamer – oligonucleotide – magnetic particle and mesoporous silica nanoparticle – aptamer – oligonucleotide – magnetic particle. However, the method for their purification from hybridisation solution resulted in low and variable yields. From the aforementioned two constructs, the former one gave better outcomes. Therefore, this construct may be chosen for the further

optimisation studies. However, it must be taken into consideration that this construct was not complete (i.e. the silica nanoparticles were lacking). Hence, the solid silica nanoparticles should be bound to superparamagnetic particles by aptamer-oligonucleotide hybrid. The resultant constructs should be magnetically purified and the yields should be compared to previously obtained yield results of mesoporous silica constructs. The outcomes of that study could give an indication whether silica nanoparticles (either porous or non-porous) hinder the hybridisation between aptamers and oligonucleotide fragments.

Binding between the aptamers and oligonucleotides may constitute a problem during hybridisation. The aptamer's complicated tertiary structure may not be unfolded sufficiently to fully hybridise to oligonucleotide fragments. Therefore, it is suggested to prepare the aptamers prior to hybridisation. This can be achieved by heating them to higher temperature or keeping them in alkaline solutions. In this way, the formation of hydrogen bonds and other interactions may be prevented.

It is also crucial to investigate the extent of aptamer binding to silica nanoparticles. This is important when establishing the capability of silica nanoparticles to carry therapeutic payload. More aptamers bound to nanoparticles would provide better means for targeting diseased cells. Therefore, silica nanoparticles should be functionalised with FITC and fluorescence spectrophotometry may measure the fluorescence of both ATTO647N as well as FITC. In this way the concentrations and yields of FITC bound to silica nanoparticles can be determined.

On a successful completion of magnetic capture-hybridisation optimisation, the aptamer-functionalised silica nanoparticles can be recovered from the solution. This may be achieved with breakage of hydrogen bonds holding aptamers and oligonucleotide sequences together.

This study showed that aptamers were indeed binding to the metastatic breast cancer cells. However, the optimal conditions for this binding were not established. Therefore, the future investigations may address this question. Perhaps a starting point for investigating optimal binding conditions between the aptamers and MCF7 cells would be to purify mucin-1 from MCF7 cells and establish the aptamer binding assay to MUC-1. If that investigation proves to be successful, the binding of aptamer-functionalised silica nanoparticles to purified mucin-1 may follow.

6 Bibliography

Alberts, B., Johnson, A., Lewis, J., Raff, M., Roberts, K. and Walter, P. (2008). *Molecular biology of the cell.* 5th ed. New York: Garland Science, Taylor & Francis Group.

Albretsen, C., Kalland, K.-H., Haukanes, B.-I., Håvarstein, L.-S. and Kleppe, K. Applications of magnetic beads with covalently attached oligonucleotides in hybridization: isolation and detection of specific measles virus mRNA from a crude cell lysate. *Analytical Biochemistry*. **189**, 40-50.

Alexis, F., Rhee, J.-W., Richie, J. P., Radovic-Moreno, A. F., Langer, R. and Farokhzad, O. C. (2008). New frontiers in nanotechnology for cancer treatment. *Urologic Oncology: Seminars and Original Investigations*. **26**, 74-85.

Amagliani, G., Omiccioli, E., del Campo, A., Bruce, I. J., Brandi, G. and Magnani, M. (2005). Development of a magnetic capture hybridization-PCR assay for *Listeria monocytogenes* direct detection in milk samples. *Journal of Applied Microbiology*. **100**, 375-383.

Bach, H.-J., Hartmann, A., Trevors, J. T. and Munch, J. C. (1999). Magnetic capture-hybridization method for purification and probing of mRNA for neutral protease of *Bacillus cereus*. *Journal of Microbiological methods*. **37**, 187-192.

Bagwe, R. P., Yang, C., Hilliard, L. R. and Tan, W. (2004). Optimization of dye-doped silica nanoparticles prepared using a reverse microemulsion method. *Langmuir*. **20**, 8336-8342.

Baines, I. C. and Colas, P. (2006). Peptide aptamers as guides for small-molecule drug discovery. *Drug Discovery Today*. **11**, 334-341.

Bartlett, J. M. S. (2002). Approaches to analysis of gene expression using mRNA. *Molecular Biotechnology*. **21**, 149-160.

Becker, H. and Gärtner, C. (2008). Polymer microfabrication technologies for microfluidic systems. *Analytical Bioanalytical Chemistry*. **390**, 89-111.

Berensmeier, S. (2006). Magnetic particles for the separation and purification of nucleic acids. *Applied Microbiology and Biotechnology*. **73**, 495-504.

Berezovski, M. V., Lechmann, M., Musheev, M. U., Mak, T. W. and Krylov, S. N. (2008). Aptamer-facilitated biomarker discovery (AptaBiD). *Journal of American Chemical Society*. **130**, 9137-9143.

Breaker, R. R. (1997). DNA aptamers and DNA enzymes. *Current Opinion in Chemical Biology*. **1**, 26-31.

Brody, E. N. and Gold, L. (2000). Aptamers as therapeutic and diagnostic agents. *Reviews in Molecular Biotechnology*. **74**, 5-13.

Cerchia, L., Hamm, J., Libri, D., Tavitian, B. and de Franciscis, V. (2002). Nucleic acid aptamers in cancer medicine. *Federation of European Biochemical Societies Letters*. **528**, 12-16.

Chen, J. and Griffiths, M. W. (2001). Detection of *Salmonella* and simultaneous detection of *Salmonella* and Shiga-like toxin-producing *Escherichia coli* using the magnetic capture hybridization polymerase chain reaction. *Letters in Applied Microbiology*. **32**, 7-11.

Cheng, J., Teply, B. A., Sherifi, I., Sung, J., Luther, G., Gu, F. X., Levy-Nissenbaum, E., Radovic-Moreno, A. F., Langer, R. and Farokhzad, O. C. (2007). Formulation of functionalized PLGA-PEG nanoparticles for in vivo targeted drug delivery. *Biomaterials*. **28**, 869-876.

Chu, T. C., Shieh, F., Lavery, L. A., Levy, M., Richards-Kortum, R., Korgel, B. A. and Ellington, A. D. (2006). Labeling tumor cells with fluorescent nanocrystal-aptamer bioconjugates. *Biosensors and Bioelectronics*. **21**, 1859-1866.

Da Pieve, C., Perkins, A. C. and Missailidis, S. (2009). Anti-MUC1 aptamers: radiolabelling with ^{99m}Tc and biodistribution in MCF-7 tumour-bearing mice. *Nuclear Medicine and Biology*. **36**, 703-710.

Darton, N. J., Sederman, A. J., Ionescu, A., Ducati, C., Darton. R. C., Gladden, L. F. and Slater, N. K. H. (2008). Manipulation and tracking of superparamagnetic nanoparticles using MRI. *Nanotechnology*. **19**, 1-5.

Dausse, E., Da Rocha Gomes, S. and Toulme, J.-J. (2009). Aptamers: a new class of oligonucleotides in the drug discovery pipeline? *Current Opinion in Pharmacology*. **9**, 602-607.

de-los-Santos-Alvarez, N., Lobo-Castanon, M. J., Miranda-Ordieres, A. J. And Tunon-Blanco, P. (2008). Aptamers as recognition elements for label-free analytical devices. *Trends in Analytical Chemistry*. **27**, 437-446.

Dupont, K., Vogensen, F. K. and Josephsen, J. (2005). Detection of lactococcal 936-species bacteriophages in whey by magnetic capture hybridisation PCR targeting a viariable region of receptor-binding protein genes. *Journal of Applied Microbiology*. **98**, 1001-1009.

Faraji, A. H. and Wipf, P. (2009). Nanoparticles in cellular drug delivery. *Bioorganic & Medicinal Chemistry*. **17**, 2950-2962.

Farokhzad, O. C., Cheng, J., Teply, B. A., Sherifi, I., Jon, S., Kantoff, P. W., Richie, J. P. and Langer, R. (2006). Targeted nanoparticles-aptamer bioconjugates for cancer chemotherapy *in vivo*. *Proceedings of the National Academy of Sciences*. **103**, 6315-6320.

Farokhzad, O. C., Khademhosseini, A., Jon, S., Hermmann, A., Cheng, J., Chin, C., Kiselyuk, A., Teply, B., Eng, G. and Langer, R. (2005). Microfluidic system for studying the interaction of nanoparticles and microparticles with cells. *Analytical Chemistry*. **77**, 5453-5459.

Ferreira, C. S. M., Matthews, C. S. and Missailidis, S. (2006). DNA aptamers that bind to MUC1 tumour marker: design and characterization of MUC1-binding single-stranded DNA aptamers. *Tumor Biology*. **27**, 289-301.

Ferreira, C. S. M., Cheung, M. C., Missailidis, S., Bisland, S. and Gariepy, J. (2009). Phototoxic aptamers selectively enter and kill epithelial cancer cells. *Nucleic Acids Research*. **37**, 866-876.

Fuentes, M., Mateo, C., Rodriguez, A., Casqueiro, M., Tercero, J. C., Riese, H. H., Fernández-Lafuente, R. and Guisán, J. M. (2006). Detecting minimal traces of DNA using DNA covalently attached to superparamagnetic nanoparticles and direct PCR-ELISA. *Biosensors and Bioelectronics.* **21**, 1574-1580.

Furlani, E. P., Sahoo, Y., Ng, K. C., Wortman, J. C. and Monk, T. E. (2007). A model for predicting magnetic particle capture in a microfluidic bioseparator. *Biomed Microdevices*. **9**, 451-463.

Gao, G.-M., Zou, H.-F., Liu, D.-R., Miao, L.-N., Ji, G.-J. and Gan, S.-C. (2009). Influence of surfactant surface coverage and aging time on physical properties of silica nanoparticles. *Colloids and Surfaces A: Physicochemical and Engineering Aspects.* **350**, 33-37.

Gu, F. X., Karnik, R., Wang, A. Z., Alexis, F., Levy-Nissenbaum, E., Hong, S., Langer, R. S. and Farokhzad, O. C. (2007). Targeted nanoparticles for cancer therapy. *NanoToday*. **2**, 14-20.

Hallmark, B., Darton, N. J., James, T., Agrawal, P. and Slater, N. K. H. (2010). Magnetic field strength requirements to capture superparamagnetic nanoparticles within capillary flow. *Journal of Nanoparticle Research*. **12**, 2951-2965.

Ho, V. H. B., Barcza, A., Chen, R., Müller, K. H., Darton, N. J. and Slater, N. K. H. (2009). The precise control of cell labelling with streptavidin paramagnetic particles. *Biomaterials*. **30**, 6548-6555.

Ho, S. B., Niehans, G. A., Lyftogt, C., Yan, P. S., Cherwitz, D. L., Gum, E. T., Dahiya, R. and Kim, Y. S. (1993). Heterogeneity of mucin gene expression in normal and neoplastic tissues. *Cancer Research*. **53**, 641-651.

Hornes, E. and Korsnes, L. (1990). Magnetic DNA hybridization of oligonucleotide probes attached to superparamagnetic bead and their use in the isolation of Poly(A) mRNA from eukaryotic cells. *GATA*. **7**, 145-150.

Huang, Y.-F., Shangguan, D., Liu, H., Phillips, J. A., Zhang, X., Chen, Y. and Tan, W. (2009). Molecular assembly of an aptamer-drug conjugate for targeted drug delivery to tumor cells. *ChemBioChem*. **10**, 862-868.

Jacobsen, C. S. and Holben, W. E. (2007). Quantification of mRNA in *Salmonella* sp. seeded soil and chicken manure using magnetic capture hybridisation PT-PCR. *Journal of Microbiological Methods.* **69**, 315-321.

James, W. (2001). Nucleic acid and polypeptide apatmers: a powerful approach to ligand discovery. *Current Opinion in Pharmacology*. **1**, 540-546.

Knopp, D., Tang, D. and Niessner, R. (2009). Review: Bioanalytical applications of biomolecules-functionalized nanometer-sized doped silica particles. *Analytica Chimica Acta*. **647**, 14-30.

Langrell, S. R. H. and Barbara, D. J. (2001). Magnetic capture hybridisation for improved PCR detection of *Nectria galligena* from lignified apple extracts. *Plant Molecular Biology Reporter*. **19**, 5-11.

Lee, J. F., Stovall, G. M. and Ellington, A. D. (2006). Aptamer therapeutics advance. *Current Opinion in Chemical Biology*. **10**, 282-289.

Levy-Nissenbaum, E., Radovic-Moreno, A. F., Wang, A. Z., Langer, R. and Farokhzad, O. C. (2008). Nanotechnology and aptamers: applications in drug delivery. *Trends in Biotechnology*. **26**, 442-449.

Li, D. and Kaner, R. B. (2005). Shape and aggregation control of nanoparticles: not shaken, not stirred. *Journal of American Chemical Society*. **128**, 968-975.

Li, N., Ebright, J. N., Stovall, G. M., Chen, X., Nguyen, H. H., Singh, A., Syrett, A. and Ellington, A. D. (2009). Technical and biological issues relevant to cell typing with aptamers. *Journal of proteome research*. **8**, 2438-2448.

Lou, X., Qian, J., Xiao, Y., Viel, L., Gerdon, A. E., Lagally, E. T., Atzberger, P., Tarasow, T. M., Heeger, A. J. and Soh, H. T. (2009). Micromagnetic selection of aptamers in microfluidic channels. *Proceedings of the National Academy of Sciences*. **106**, 2989-2994.

Lu, Y. and Liu, J. (2006). Functional DNA nanotechnology: emerging applications of DNAzymes and aptamers. *Current Opinion in Biotechnology*. **17**, 580-588.

Lund-Olsen, T., Bruus, H. and Hansen, M. F. (2007). Quantitative characterization of magnetic separators: Comparison of systems with and without integrated microfluidic mixers. *Biomed Microdevices*. **9**, 195-205.

Mader, H., Li, X., Saleh, S., Link, M., Kele, P. and Wolfbeis, O. S. (2008). Fluorescent Silica Nanoparticles. *Annals of the New York Academy of Sciences.* **1130**, 218-223.

McCarthy, J. R. and Weissleder, R. (2008). Multifunctional magnetic nanoparticles for targeted imaging and therapy. *Advanced Drug Delivery Reviews*. **60**, 1241-1251.

Mishra, B., Patel, B. B. and Tiwari, S. (2010). Colloidal nanocarriers: a review on formulation technology, types and applications toward targeted drug delivery. *Nanomedicine: Nanotechnology, Biology, and Medicine*. **6**, 9-24.

Miyatake, T., MacGregor, B. J. and Boschker, H. T. S. (2009). Linking microbial community function to phylogeny of sulfate-reducing *Deltaproteobacteria* in marine sedimants by combining stable isotope probing with magnetic-bead capture hybridization. *Applied and Environmental Microbiology*. **75**, 4927-4935.

Ng, E. W. M., Shima, D. T., Calias, P., Cunningham, Jr., E. T., Guyer, D. R. and Adamis, A. P. (2006). Pegaptanib, a targeted anti-VEGF aptamer for ocular vascular disease. *Nature Reviews/Drug Discovery*. **5**, 123-132.

Nimjee, S. M., Rusconi, C. P. and Sullenger, B. A. (2005). Aptamers: an emerging class of therapeutics. *Annual Review in Medicine*. **56**, 555-583.

Osborne, S. E., Matsumura, I. and Ellington, A. D. (1997). Aptamers as therapeutic and diagnostic reagents: problems and prospects. *Current Opinion in Chemical Biology*. **1**, 5-9.

Park, S. K., Kim, K. D. and Kim, H. T. (2002). Preparation of silica nanoparticles: determination of the optimal synthesis conditions for small and uniform particles. *Colloids and Surfaces A: Physicochemical and Engineering Aspects*. **197**, 7-17.

Pestourie, C., Tavitian, B. and Duconge, F. (2005). Aptamers against extracellular targets for in vivo applications. *Biochimie*. **87**, 921-930.

Phillips, J. A., Lopez-Colon, D., Zhu, Z., Xu, Y. and Tan, W. (2008). Applications in aptamers in cancer cell biology. *Analytica Chmica Acta*. **621**, 101-108.

Rao, K. S., El-Hami, K., Kodaki, T., Matsushige, K. and Makino, K. (2005). A novel method for synthesis of silica nanoparticles. *Journal of Colloid and Interface Science*. **289**, 125-131.

Pestourie, C., Tavitian, B. and Duconge, F. (2005). Aptamers against extracellular targets for in vivo applications. *Biochimie*. **87**, 921-930.

Phillips, J. A., Lopez-Colon, D., Zhu, Z., Xu, Y. and Tan, W. (2008). Applications in aptamers in cancer cell biology. *Analytica Chmica Acta*. **621**, 101-108.

Rao, K. S., El-Hami, K., Kodaki, T., Matsushige, K. and Makino, K. (2005). A novel method for synthesis of silica nanoparticles. *Journal of Colloid and Interface Science*. **289**, 125-131.

Robinson, D. B., Persson, H. H. J., Zeng, H., Li, G., Pourmand, N., Sun, S. and Wang, S. X. (2005). DNA-functionalized MFe_2O_4 (M = Fe, Co, or Mn) nanoparticles and their hybridisation to DNA-functionalized surfaces. *Langmuir*. **21**, 3096-3103.

Ruddon, R. W. (2007). *Cancer Biology*. 4th ed. Oxford: Oxford University Press.

Sampson, T. (2003). Aptamers and SELEX: the technology. *World Patent Information*. **25**, 123-129.

Safarik, I. and Safarikova, M. (2004). Magnetic techniques for the isolation and purification of proteins and peptides. *Biomagnetic research and technology*. **2**.

Saiyed, Z. M., Telang, S. D. and Ramchand, C. N. (2003). Application of magnetic techniques in the field of drug discovery and biomedicine. *BioMagnetic Research and Technology*. **1**.

Smith, J. E., Medley, C. D., Tang, Z., Shangguan, D., Lofton, C. and Tan, W. (2007). Aptamer-conjugated nanoparticles for the collection and detection of multiple cancer cells. *Analytical Chemistry*. **79**, 3075-3082.

Smith, J. E., Wang, L. and Tan, W. (2006). Bioconjugated silica-coated nanoparticles for bioseparation and bioanalysis. *Trends in Analytical Chemistry*. **25**, 848-855.

Tartaj, P., Morales, M. P., Gonzalez-Carreno, T., Veintemillas-Verdaguer, S. and Serna, C. J. (2005). Advances in magnetic nanoparticles for biotechnology applications. *Journal of Magnetism and Magnetic Materials*. **290-291**, 28-34.

Thompson, D. E., Rajal, V. B., De Batz, S. and Wuertz, S. (2006). Detection of *Salmonella* spp. in water using magnetic capture hybridisation combined with PCR or real-time PCR. *Journal of Water and Health.* **4**, 67-75.

Tombelli, S., Minunni, M. and Mascini, M. (2005). Analytical applications of aptamers. *Biosensors and Bioelectronics*. **20**, 2424-2434.

Tong, R., Yala, L., Fan, T. M. and Cheng, J. (2010). The formulation of aptamer-coated paclitaxel-polylactide nanoconjugates and their targeting to cancer cells. *Biomaterials*. **31**, 3043-3053.

Tothill, I. E. (2009). Biosensors for cancer marker diagnosis. *Seminars in Cell & Developmental Biology*. **20**, 55-62.

Townley, H. E., Parker, A. R. and White-Cooper, H. (2008). Exploitation of diatom frustules for nanotechnology: tethering active biomolecules. *Advanced Functional Materials*. **18**, 369-374.

Veiseh, O., Gunn, J. W. and Zhang, M. (2010). Design and fabrication of magnetic nanoparticles for targeted drug delivery and imaging. *Advanced Drug Delivery Reviews*. **62**, 284-304.

Wang, Y., Wang, Y. and Liu, B. (2008). Fluorescent detection of ATP based on signaling DNA aptamer attached silica nanoparticles. *Nanotechnology*. **19**, 1-6.

Whitesides, G. M., Kazlauskas, R. J. and Josephson, L. (1983). Magnetic separations in biotechnology. *Trends in Biotechnology*. **1**, 144-148.

Xu, H., Yan, F., Monson, E. E. and Kopelman, R. (2003). Room-temperature preparation and characterization of poly(ethylene glycol)-coated silica nanoparticles for biomedical applications. *Journal of Biomedical Materials Research*. **66A**, 870-879.

Appendix

Table A.1. Fluorescence intensity values (a.u.) for various aptamer solution concentrations at gain 2900.

Plate reader measurement number	Aptamer concentration [nM] at gain 2900							
	100	75	50	10	1	0.1	0.01	0
1	228536	146235	99817	26037	6369	3996	4002	4255
2	217450	147658	97202	24774	6027	4912	3264	3888
3	222092	140767	93638	26526	5990	4503	4658	3528
Mean	222693	144887	96886	25779	6129	4470	3975	3890
SD	5567	3638	3102	904	209	459	697	364

Table A.2. Fluorescence intensity (a.u.) of ATTO647N for various aptamer concentrations at gain 2800.

Plate reader measurement number	Aptamer concentration [nM] at gain 2800							
	100	75	50	10	1	0.1	0.01	0
1	168139	109435	74399	19969	4926	3297	3301	2758
2	166482	111137	71569	19206	4586	2638	3453	2977
3	172272	106112	71225	18762	4474	2809	3093	2967
Mean	168964	144887	72398	19312	4662	2915	3282	2901
SD	2982	3638	1742	610	235	342	181	124

Table A.3. Fluorescence intensity (a.u.) of ATTO647N for various aptamer concentrations at gain 3500.

Plate reader measurement number	Aptamer concentration [nM] at gain 3500							
	150	100	75	50	25	10	1	0
1	61738	39877	31934	21751	11286	5065	1406	1312
2	60654	39955	31178	21568	10110	5015	1376	1422
3	59281	41399	31394	21877	10929	4984	1262	1162
4	56694	39938	33785	21338	11065	4730	1659	1429
5	58962	39399	32124	22089	11125	4543	1254	1370
6	57593	19485	24270	18285	9121	4068	1360	1215
Mean	59152	40114	32083	21725	10903	4867	1386	1383
SD	1871	754	1026	288	461	223	147	54

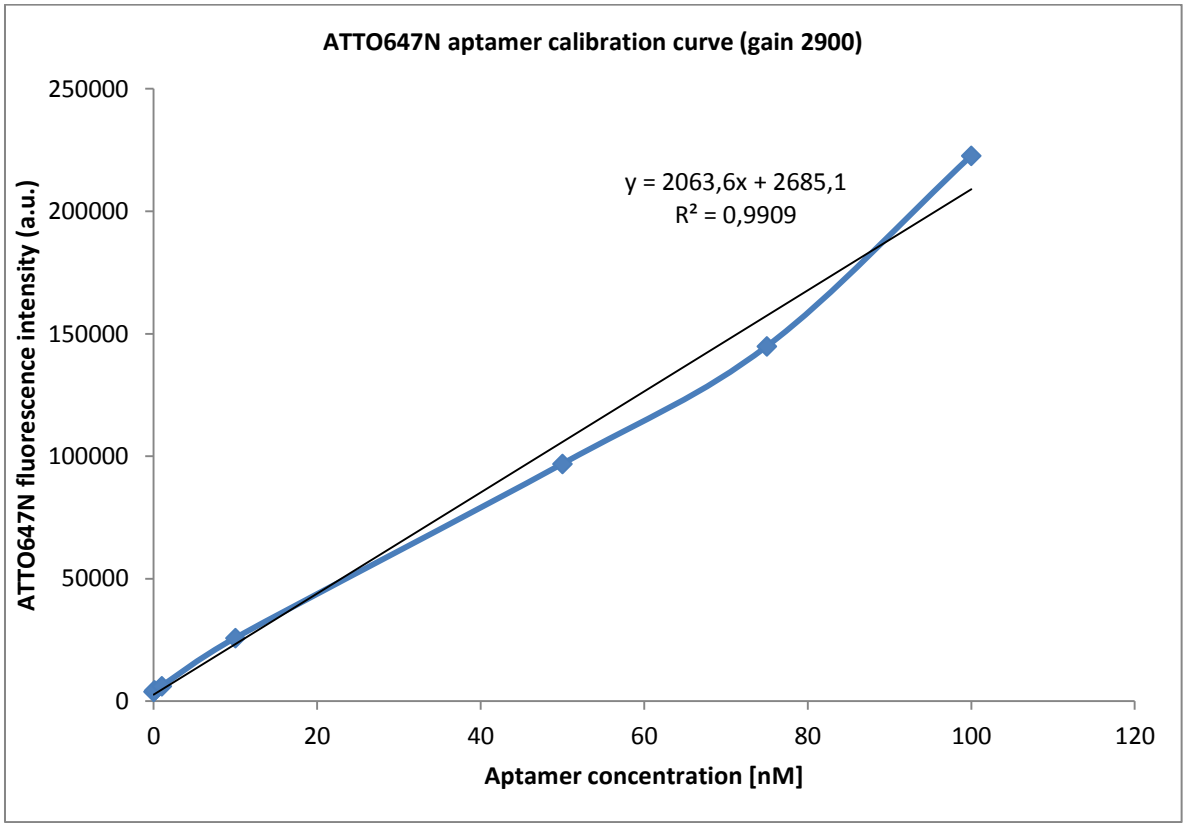

Figure A.4. Calibration curve of ATTO647N fluorescence intensity versus aptamer concentration.

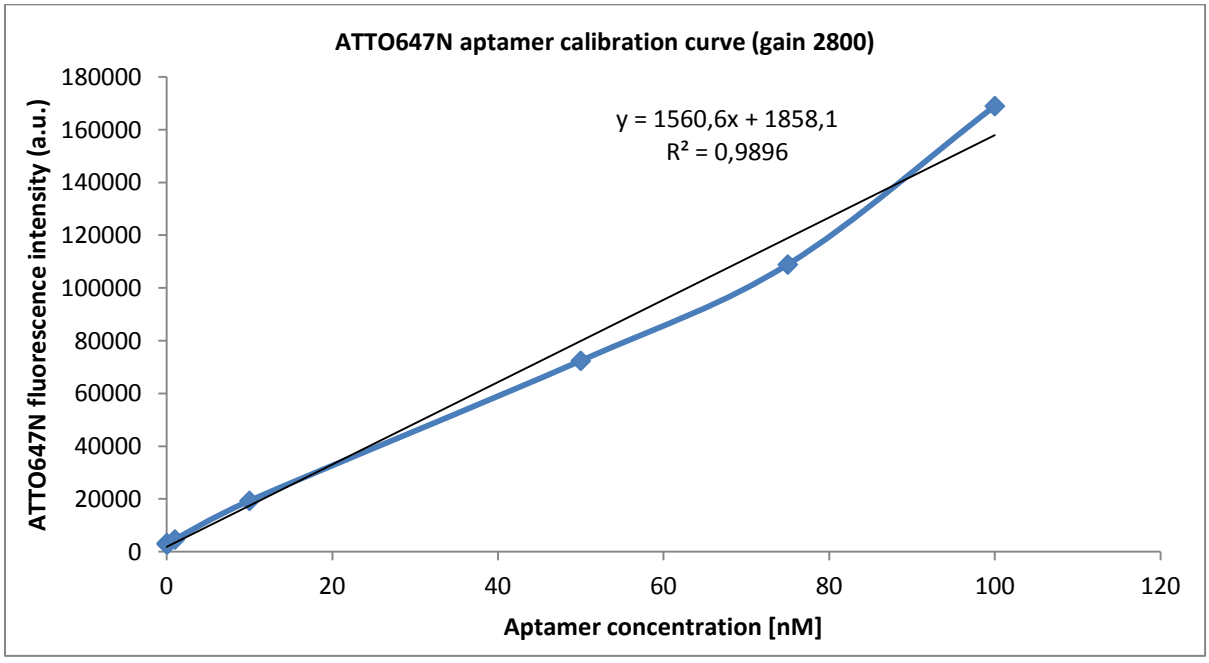

Figure A.5. Calibration curve of ATTO647N fluorescence intensity versus aptamer concentration.

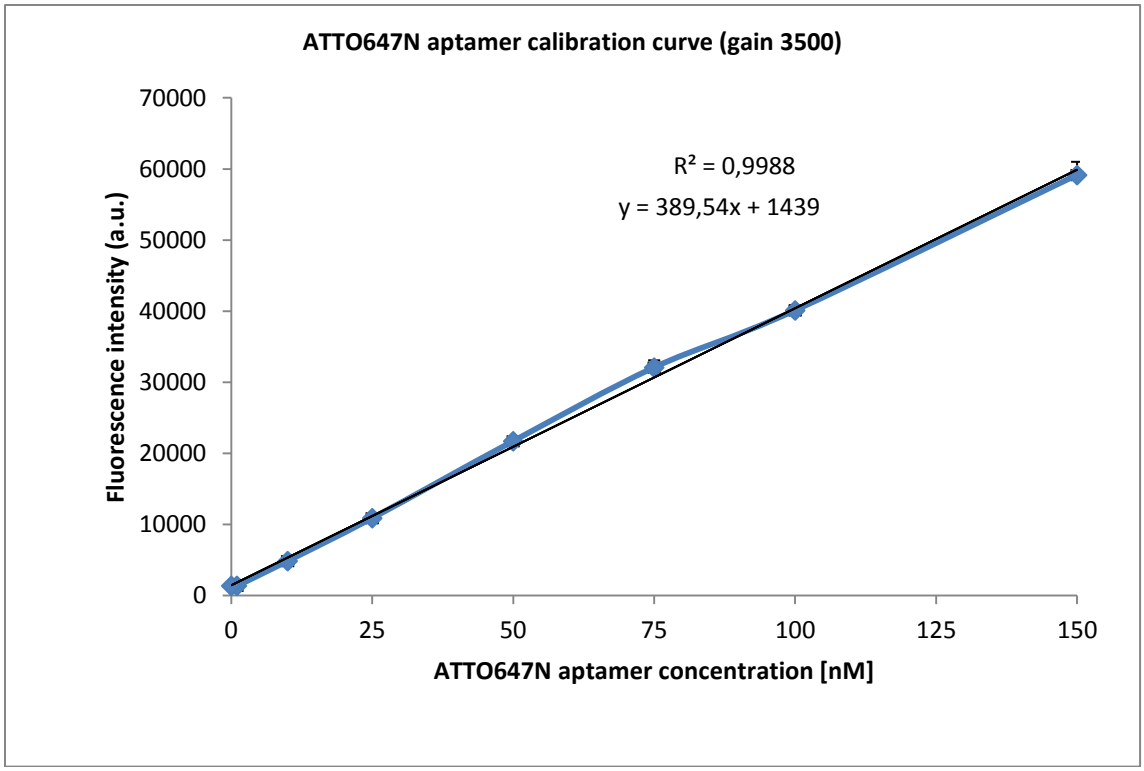

Figure A.6. Calibration curve of ATTO647N fluorescence intensity versus aptamer concentration.

Table A.7. Experimental conditions under which the zeta potential of solid silica nanoparticle dispersion was measured.

pH	Zeta Potential [mV]	Temperature [°C]	Mobility [µmcm/Vs]	Conductivity [mS/cm]
3	-11.9	22.0	-0.09	0.63
4	-21.3	22.0	-1.58	0.03
5	-50.7	22.1	-3.74	0.02
5.5	-49.9	22.0	-3.69	0.02
6	-49.0	22.0	-3.63	0.04
6.5	-50.6	22.0	-3.74	0.04
7	-54.6	22.0	-4.04	0.04
7.5	-52.5	21.9	-3.88	0.06
8	-35.8	22.1	-2.65	0.12
9	-21.0	22.0	-1.56	3.02